New benzene absorption cross sections in the VUV, relevance for Titan's upper atmosphere

Fernando J. Capalbo, Yves Bénilan, Nicolas Fray, Martin Schwell, Norbert Champion, Et-Touhami Es-Sebbar, Tommi T. Koskinen, Lehocki Ivan, Roger V. Yelle

New benzene absorption cross sections in the VUV, relevance for Titan's upper atmosphere

F.J. Capalbo[a,*], Y. Bénilan[a], N. Fray[a], M. Schwell[a], N. Champion[b,c], Et. Es-sebbar[a], T.T. Koskinen[d], I. Lehocki[a], R.V. Yelle[d]

[a] *Laboratoire Interuniversitaire des Systèmes Atmosphériques (LISA), UMR CNRS 7583, University Paris-Est Créteil (UPEC) and University Paris Diderot (UPD), 61 avenue du Général de Gaulle, 94010, Créteil, France*
[b] *LERMA, Observatoire de Paris, PSL Research University, CNRS, UMR 8112, F-92190, Meudon, France*
[c] *Sorbonne Universités, UPMC Univ. Paris 6, UMR 8112, LERMA, F-75005, Paris, France*
[d] *Lunar and Planetary Laboratory, University of Arizona, AZ 85721, Tucson, USA*

Abstract

Benzene is an important molecule in Titan's atmosphere because of its potential to be intermediate between the gas phase and the organic solid phase. We measured photoabsorption in the ultraviolet by benzene gas at temperatures covering the range from room temperature to 215 K. We derived benzene absorption cross sections and analyzed them in terms of the transitions observed. No significant variation with measurement temperature was observed. We discuss the implications of our measurements for the derivation of benzene abundance profiles in Titan's thermosphere, by the Cassini/Ultraviolet Imaging Spectrometer (UVIS). The use of absorption cross sections at low temperature is recommended for the analysis. We used our measurements, together with absorption cross sections from other molecules, to analyze four stellar occultations by Titan, measured by UVIS during flybys T21, T41, T41_II, and T53. We derived and compared benzene abundance profiles in Titan's thermosphere between approximately 530 and 1000 km, for different dates and geographical locations. The comparisons of our benzene profiles with each other, and with profiles from models of the upper atmosphere, point to a complex behavior, out of reach by current photochemical models.

Keywords:
Spectroscopy, Ultraviolet observations, Titan, atmosphere, Occultations, Atmospheres, composition, Astrobiology

*Corresponding author

1. Introduction

Titan's atmosphere is a rich reservoir of complex organic molecules. The identification and characterization of these molecules have been pursued with theoretical modeling of the atmosphere, laboratory experiments reproducing atmospheric conditions, and observations of the atmosphere itself. Among the complex hydrocarbons obtained in the models, experiments, and observed, is C_6H_6. From all the possible isomers with this elemental formula, this work deals with the cyclic form, c-C_6H_6, called benzene. Apart from its detection in Titan (Coustenis et al., 2003), benzene was also detected in Jupiter, Saturn (Bézard et al., 2001) and in the CRL618 nebula from ISO data (Cernicharo et al., 2001). It is the simplest of the aromatic hydrocarbons: a group of hydrocarbons characterized by alternating double and single bonds between carbons. Benzene is a potential precursor to the formation of a whole host of heavier hydrocarbons, including polycyclic aromatic hydrocarbons (PAHs) and polyphenyls (Delitsky and McKay, 2010). The condensation of these aromatic compounds may contribute to the formation of Titan's haze layers (Wilson et al., 2003; Wilson and Atreya, 2003; Lebonnois, 2005). As a consequence benzene is one of the most interesting molecules detectable in Titan's atmosphere. In the remainder of this section we review the observations and models of benzene chemistry on Titan, as well as provide an overview of the previous measurements of its Vacuum Ultraviolet (VUV) absorption cross section.

1.1. Benzene on Titan

After the detection of benzene among the products of laboratory experiments simulating Titan's atmospheric chemistry (see for example Sanchez et al., 1966; Raulin et al., 1982; Coll et al., 1999; Imanaka et al., 2010), chemical models started to include this molecule. For example, motivated by the detection of polyaromatic compounds in laboratory tholins and theoretical work based on PAHs formation from benzene, Lebonnois et al. (2002) included it in their model for Titan's atmosphere and suggested chemical pathways that can link this simple molecule and PAHs to macromolecules, precursors to aerosol particles. However, this aerosol formation pathway was negligible in their model compared to others pathways (polymers of acetylene, polymers of HCN). This might be due to underestimated reaction rates, or to the low quantities of benzene in their model, small compared to the measured abundances given in Coustenis et al. (2003), derived from Infrared Space Observatory (ISO) spectra. These measurements constituted the first identification of benzene in Titan's atmosphere, with a mole fraction of $(4 \pm 3)\times10^{-10}$ in the stratosphere. The detection

of benzene triggered more attempts to model its production, and the inclusion of PAHs in the models for aerosol formation, particularly because of their importance as intermediate link in the gas-aerosol path, and haze formation. Wilson et al. (2003) analyzed mechanisms for the formation of benzene based on recombination of the propargyl radical (C_3H_3) and compared their results with the ISO observations. They found that ion chemistry plays a significant role on the formation of benzene above 750 km. The modeled benzene profile was updated in subsequent works (Wilson and Atreya, 2003, 2004), providing a better fit to the ISO measurements. Lebonnois (2005) presented a sensitivity study of c-C_6H_6 and PAHs on both Titan and Jupiter. In this model benzene was mostly produced by recombination of the propargyl radicals (C_3H_3), the benzene abundance was higher than that predicted by Lebonnois et al. (2002), and the PAH pathway was comparable to the other pathways considered for aerosol formation. The revised model agreed with the ISO measurements, the only observational constraints available at that time.

After the Cassini arrival to Saturn in 2004, observations provided stronger constraints on the models. The presence of benzene in the stratosphere was confirmed by Coustenis et al. (2007) and Vinatier et al. (2007) using data from the Composite InfraRed Spectrometer (CIRS). The first of these references is based on nadir observations, and does not provide vertical profiles of the detected species. It presented an analysis of data from a Titan northern winter period, in which benzene was found to increase in abundance from some 3×10^{-10} at the equator to a maximum abundance of $(3.5 \pm 2.5) \times 10^{-9}$ at 70° N. The first vertical profile in the stratosphere was provided by Vinatier et al. (2007). Limited to 80° N during northern winter, the abundance increases with altitude from 3 $\times 10^{-9}$ (at about 160 km) to 5×10^{-9} (at about 320 km), although with overlapping uncertainties. They also provided an upper limit for c-C_6H_6 abundance of 1.1×10^{-9} in the southern hemisphere. Higher in the atmosphere (> 900 km) measurements with the Ion and Neutral Mass Spectrometer (INMS) (Waite et al., 2005; Vuitton et al., 2006, 2007; Cui et al., 2009), from several Cassini flybys, resulted in benzene abundances some orders of magnitude bigger than the models predicted. Unexpectedly high abundances of other complex hydrocarbons were also derived. In this way, Cassini observations added new information about the benzene abundances at low altitudes, and provided new constraints to the interpretation of its profile in the upper thermosphere.

The new observations were readily applied to improve the photochemical models. In their analysis of INMS data, Vuitton et al. (2007) provided a c-C_6H_6 mole fraction in the thermosphere derived from measured abundance of protonated benzene. They found higher concentrations in

the thermosphere than previous results, which they associated to a production mechanism in the higher layers. On the other hand, the predictions of Lavvas et al. (2008) are below INMS results. For Lavvas et al. (2008) the main production process for benzene in the upper atmosphere was the recombination of two C_3H_3 radicals. Their analysis did not include the full ion chemistry that Vuitton et al. (2008) found to be critical for explaining high benzene densities. Vuitton et al. (2008) presented a detailed study on the formation and distribution of c-C_6H_6 in Titan, using an ion chemistry model and a neutral chemistry model to analyze the production mechanisms in the atmosphere. The results were validated by comparison with INMS measurements from 12 flybys in the upper atmosphere and with CIRS values for the stratosphere. Vuitton et al. (2008), like Vuitton et al. (2007), suggested a main source of benzene in the thermosphere, where it is created mainly by ion chemistry. These last works significantly improved the understanding of ion chemistry in Titan's atmosphere, and were followed in subsequent studies. De La Haye et al. (2008) developed a 1D ion-neutral rotating model to account for diurnal variations of solar irradiation. In their model two main processes are responsible for benzene production: neutral chemistry of C_3H_3 below 700 km, and electron recombination of $C_6H_7^+$ above 700 km. This last production mechanism is dominant in the thermosphere, as in Vuitton et al. (2008). In line with most of the recent studies, Krasnopolsky (2009), in their photochemical model of coupled neutral and ion chemistry of Titan, also favored ion chemistry over neutral chemistry for the formation of PAH in the upper atmosphere. Therefore, the latest studies suggest that the neutral pathway dominates in the upper stratosphere and mesosphere, while the ion chemistry pathway is important in the thermosphere.

Despite the agreement on the formation of benzene and other heavy molecules in the upper atmosphere of Titan, the detailed chemistry of benzene and other heavy species, and their role in forming organic molecules and aerosols, is still poorly understood. The profiles from the photochemical models have associated a big uncertainty (Hebrard et al., 2007), and change dramatically as a function of the chemical reactions involved. New atmospheric observations can help to solve the problems in the models. But the observations from Cassini/CIRS that probe the lower atmosphere are limited to altitudes below 300 km, while Cassini/INMS measurements of benzene in the thermosphere are limited to altitudes above 950 km. This leaves an important gap in the mesosphere, which is the transition region between the neutral and ion pathways to the formation of benzene, and a site of accelerated aerosol growth. Fortunately, this region can be probed by stellar occultations measured in the Far Ultraviolet (FUV) channel of the Cassini/UVIS instrument during Titan

flybys. Koskinen et al. (2011) presented the first identification of benzene in this region based on the UVIS data, and provided two preliminary density profiles for flybys T41 and T53. These results were obtained by using the first release of the c-C_6H_6 absorption cross sections, measured at room temperature, resulting from the laboratory measurements presented in Section 2. Here we present revised density profiles of benzene for the two occultations analyzed previously by Koskinen et al. (2011), this time with an updated, low temperature, set of absorption cross sections for benzene (Section 3). In addition, we include new density profiles of benzene for two more occultations from flybys T21 and T41. We note that the study of more occultations, corresponding to different spatial/temporal coordinates, would facilitate the assessment of the variability and trends in the density profiles. Unfortunately, many of the Titan stellar occultations suffer from severe pointing drifts. The four presented here are, to the best of our knowledge, all of the stable occultations that benzene could be retrieved from prior to 2014.

1.2. Introduction to benzene absorption cross sections in the VUV

To interpret atmospheric absorption measured from stellar occultations, one needs quantitative absorption spectra of the molecules of interest. Unfortunately, the absorption cross section spectra for many molecules of planetological interest are unknown, or poorly known. The absorption spectrum of benzene is an exception, since its interpretation has served as a benchmark for the development and testing of theoretical approaches to describe π-electron systems for a long time. The absorption spectrum also provides useful information in a large number of scientific contexts, including studies in aeronomy, astrophysics, planetary science, radiation chemistry, physics, and biology. Numerous experimental and theoretical studies have been carried out, particularly in the VUV spectral region. Some of these experiments will be reviewed here in order to provide a context to our own measurements, however we do not pretend to give a full bibliographical review. In some cases, published studies give no comments about resolution, uncertainties or the temperature (we assume 298 K) used in the experiments. For more details, the reader is also referred to the bibliography found within the references cited here.

The first measurements of VUV absorption of benzene were reported by Price and Wood (1935), who photographed the absorption spectra of C_6H_6 and C_6D_6 in the wavelength range 1000 - 2000 Å. They identified Rydberg transitions in the short wavelength region for the first time, but mention only marginally the big absorption feature around 1800 Å. (Price and Walsh, 1947) investigated this region and identified tentatively at least two electronic transitions in the 1600 - 2000 Å region.

These early studies do not present absolute absorption cross sections as a function of wavelength. These were provided for the first time by Pickett et al. (1951), who used a photographic method to determine absolute values of extinction coefficients measured in the range 1560 - 2200 Å. Their analysis of the temperature variation of some of the bands in the 2000 Å band system found no measurable difference between spectra at room temperature, and those measured at ∼253 K. Hammond and Price (1955) used a photoelectric detector to determine absorption cross sections in the range 1650 - 2150 Å. From the plots in these last two cited studies, both resolutions are coarse compared to the present study (see Section 2). Wilkinson (1956) obtained higher-resolution (0.026 to 0.065 Å) absorption spectra of benzene and deuterated benzene in the VUV. They used a more appropriate continuum as radiation source, that facilitated the identification of many new weak bands with respect to Price and Wood (1935). Koch and Otto (1972) used spectrally continuous synchrotron radiation from the DESY electron accelerator, to measure benzene absorption cross sections in the photon energy range of 6 - 35 eV (350 - 2060 Å), with a wavelength resolution between 1 and 4 Å. In their work they noted assigned Rydberg states, vibrational structures, and reviewed first ionization energy values available at that time. Pantos et al. (1978) measured benzene extinction coefficients at room temperature, from 1350 - 2700 Å, at several resolutions. The resolution of the spectrum showed in their work is 2.5 Å. Their extinction measurements, that have been widely used in the literature, have an uncertainty of 10%. These are just some of the studies that set the first steps in interpreting the VUV absorption of benzene.

By the end of the 20th century, new experimental techniques and theoretical studies allowed to further investigate the absorption in the UV and review old interpretations. Grubb et al. (1985) performed four-photon absorption spectroscopy measurements. They reported several Rydberg series in the benzene spectrum converging to the first ionization energy. Suto et al. (1992) also measured benzene absorption cross sections in the 1060-2950 Å range, at 1 Å resolution and room temperature (297 K). Their results agree with those from Pantos et al. (1978), within the 10% uncertainty in the newer results. Many other studies performed in the '80s and '90s were referred to by Rennie et al. (1998), who measured absolute photoabsorption, photoionization, and photodissociation cross-sections, and the photoionization quantum efficiency of benzene and hexadeuterobenzene, in the range 350 - 1300 Å. The resolution ranged from 1.7 to 2.3 Å in the range 1160 - 1340 Å. Rennie et al. (1998) used the Pantos et al. (1978) and other authors' measurements to make a composite spectrum, including the whole range covered by our measurements (and even shorter wavelengths).

Feng et al. (2002) presented absolute UV and VUV photoabsorption oscillator strengths (cross sections), for the valence shell discrete and continuum regions of benzene from 4 to 56 eV (approximately 3100 - 220 Å), using dipole (e,e) spectroscopy, with an uncertainty of at most 5%. They provided a summary of the available absolute photoabsorption cross sections of benzene at different energy ranges, as well as a thorough comparison with previous results.

In this work we present new measurements of the c-C_6H_6 absorption cross section in the region 1160 - 2200 Å, at a resolution of 1 Å, including its dependence on temperature (mainly in 1700 - 1900 Å) . To our knowledge, this temperature dependence has not been reported previously. Our absorption measurements are described in Section 2, our results and their analysis in Section 3. We used our absorption cross sections for the detection of benzene in Titan with UVIS, using stellar occultations measured in its FUV range (1115 - 1900 Å). This technique and the UVIS data reduction are briefly described in Section 4. Benzene abundances in Titan's upper atmosphere will be presented in Section 5. Finally, Section 6 provides overall conclusions.

2. Experimental measurements of benzene absorption cross section

The absorption cross sections where derived from absorption measurements of c-C_6H_6 gas contained in a closed cell, illuminated with VUV radiation. The sample used was the product 109646 from Merck, reference substance for gas chromatography with a stated purity of better than 99.9%. No impurities were detected in any of the measurements performed. The pressure and the temperature in the cell were continuously monitored and controlled. Some of the measurements were performed at the synchrotron facility BESSY II , Berlin, Germany; others with the 10 m VUV spectrograph at the Paris Observatory, Meudon, France. The different setups and procedures are described in the next subsections. More detailed information can be found in Capalbo (2014).

2.1. Absorption measurements with Synchrotron radiation, BESSY II facility

Synchrotron radiation (SR) from an electron storage ring is a spectrally continuous and well collimated light source for spectroscopy. It can be used in different wavelength ranges, including VUV. The experimental setup and schematics have been described by Ferradaz et al. (2009). A solid benzene sample was contained in a glass tube at liquid nitrogen temperature, connected to the absorption cell through a vacuum line. The sample vapor was introduced into the cell, by sublimation and irradiated with SR from the BESSY II storage ring (Berlin-Adlershof) using the

3-m normal incidence monochromator (NIM) dipole beamline. Measurements were performed in the 1150 - 2200 Å range, at 1 Å resolution and 3 points per resolution interval. The resolution used is sufficient for the application to the analysis of UVIS spectra (with a resolution of ∼2.4 Å). The wavelength values have a varying precision depending on the wavelength region studied, being of 0.17 Å in the worst case. The absolute accuracy of the monochromator was found to be of about 3 Å at this beamline. The SR spectra were solid shifted with respect to the spectra measured in Meudon (see below), the latter calibrated using the Schumman-Runge dioxygen absorption bands. High energy stray light from the source was minimized by refocalization and strong collimation of the monochromatized beam. The absorption cell was placed as close as practically possible to the focus of the refocalizing mirror. The volume of the cylindrical cell was about 950 cm^3. The effective optical path of the cell was 14.15 cm. The entrance and exit of the cell were covered by LiF and MgF_2 windows, respectively. This allowed measurements down to the MgF_2 cutoff wavelength (about 1140 Å). The intensity of the beam at the exit of the cell was measured with an Electron Tubes Ltd 9402B solar blind photomultiplier (PM). The separate PM chamber was evacuated too, and held at room temperature. A cold-cathode pressure gauge was used to check the stability of the empty cell base pressure ($\sim 10^{-2}$ μbar). The cell pressure was measured using 2 capacitance sensor gauges (MKS 127AA): one measured absolute pressure in the range up to 1 mbar, the other in the range up to 1000 mbar. The range of c-C_6H_6 pressure used was 6 - 375 μbar, much lower than the saturation pressure at the temperatures used (e.g. ∼1000 μbar at 230 K). The static pressure increased a few μbar during the measurements due to air leaks, but this had a negligible effect on the experiment.

The temperature was controlled during the low temperature part of the experiment using a liquid nitrogen flow through the jacket that surrounds the cell. This flow was regulated by a cryogenic valve steered with a proportional, integral, derivative (PID) controller, in charge of keeping the system at a desired temperature. This latter quantity was measured with two type-K thermocouples fixed on the inside wall of the cell, and located at the opposite flat plates of the cylinder. The temperature variation during a measurement was about ±2 K, due to liquid nitrogen injection cycles. The temperature gradient across the cell was about 15 K. The values given for low temperature measurements correspond to an average value.

A measurement series to obtain one c-C_6H_6 absorption spectrum at a particular temperature, wavelength range, and pressure, was performed as follows. First an empty cell spectrum was

measured. Then the chamber was filled with c-C_6H_6 to a desired pressure. After the measurement of the sample spectrum, a second empty cell spectrum was measured. Taken at a base pressure of $10^{-2}\mu$bar of residual air, these vacuum spectra were measured with 0.5 or 0.3 points per resolution to save measurement time, and interpolated during processing to match the sampling of the benzene spectra. During the measurements, the ring current in the storage ring, and consequently the intensity of the radiation beam, diminished with time between electron injections, and was recorded during the measurement. Taking this into account, a vacuum spectrum was estimated, interpolating between the two recorded vacuum spectra. Transmission was determined from the ratio of the benzene and the calculated vacuum intensities, the absorption cross section was derived from this transmission (see below).

Different series of absorption cross section spectra were measured in this experiment. These series covered different wavelength ranges, and different temperatures. Moreover, several measurements were performed varying only the pressure, to confirm reproducibility and pressure independence of the results. A total of 36 spectra were collected. Ten of them were discarded due to experimental problems (very low absorption, low signal - to - noise ratio (S/N), etc). The resulting 26 spectra were arranged in sets, each composed of spectra measured with different pressures and wavelength ranges, but the same temperature. Absorption cross section values in each set were averaged in the wavelength regions where they overlapped. The resulting spectra are listed in Table 3.

2.2. Absorption measurements with a deuterium lamp source, Paris Observatory facility

The set up for this experiment is shown in Figure 1. The liquid sample at equilibrium vapor pressure, was contained in a glass tube at room temperature, connected to the absorption cell through a vacuum line. The sample vapor was introduced into the cell prior to the absorption measurements. Radiation from a Heraeus D200 VUV deuterium (^{2}H) lamp was used as a continuum source. The non-collimated radiation enters directly the sample chamber through its few-centimeter aperture. This means the molecules were irradiated with a VUV radiation flux from 1140 to 4000 Å modulated in intensity according to the relative radiance spectrum of the lamp, and the transmission of the windows. This motivated the presence of a shutter valve between the source and the absorption cell to minimize photochemical degradation during sample injection. All measurements were performed in the 1710 - 1910 Å range, with a relative resolution ($\lambda/\Delta\lambda$) of 2000, and 7 points per resolution interval. The vacuum spectra were measured at the same resolution and sampling as the benzene

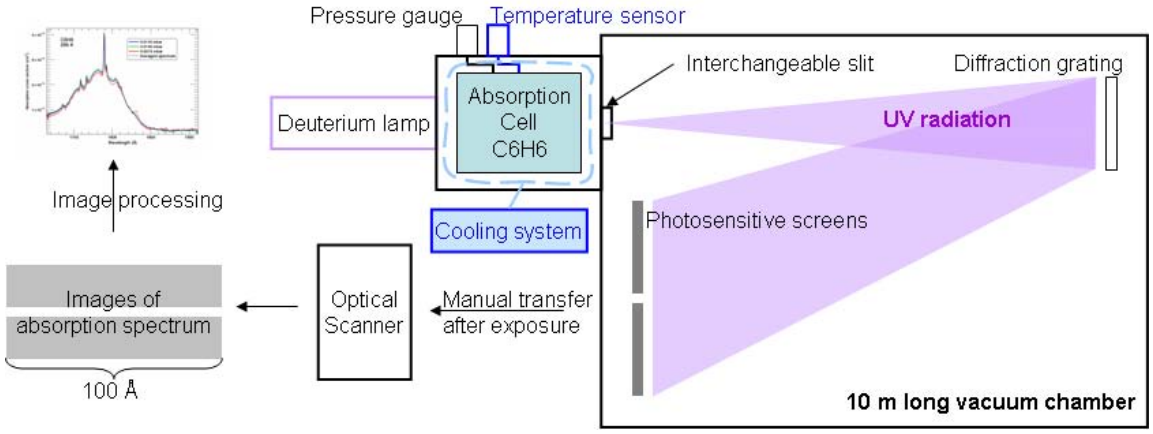

Figure 1: Experimental setup used to measure benzene absorption cross section with a deuterium lamp as a source, at the Paris Observatory facility.

spectra. The choice of these values was a compromise between resolution and exposure time of the sensitive image plates, where the spectra were registered. The wavelength scale was calibrated using the Schumann-Runge dioxygen absorption bands (see below), and is accurate to (1 - 6)$\times 10^{-2}$ Å. The lamp intensity was variable along the entrance slit, and wavelength dependent. Therefore, the measurements of a same day were performed using the same region of the lamp profile. The source also presented a flux variation of about 0.1%/min, limiting exposure time. Given the configuration of the experiment, no stray light was expected from the environment.

The absorption cell was the same as for the BESSY II measurements, this time closed with two MgF_2 windows. The experiment configuration in this case resulted in an optical path for the radiation of 17.45 cm. After leaving the absorption cell, the beam passed an interchangeable slit (2 mm for measurements at a relative resolution of 2000) and reached a 3600 lines/mm reflective concave diffraction grating, in a Rowland Circle configuration with a diameter of 10.7 m. The spectrograph has an Eagle in-plane mounting where the slit and the plate holder for detection are in the same plane. The grating and the plate holder have to be rotated and displaced to keep the image in focus when the wavelength range is changed. The spectrum was recorded simultaneously on 2 FUJI photosensitive plates, each of them having a maximum useful length of 38 cm, and linear response in intensities over five orders of magnitude. The photosensitive plates integrate the received flux, so unstable or pulsed emission light sources can be used. The characteristics of the

spectrograph are summarized in Table 1. It is worth noting the similarities between this instrument concept and the UVIS instrument in Cassini, the latter being, roughly, a reduced space version of the former.

Table 1: Characteristics of the 10 m spectrograph at Paris Observatory.

Grating	holographic (Jobin-Yvon)
Radius of the grating, m	10.685
Number of lines/mm	3600
λ of maximum efficiency, Å	1200
Plate factor (linear dispersion on the plate), Å/mm	0.25
$\lambda/\Delta\lambda$	2000, 50000, 150000
Wavelength range, Å	250 - 2200, with image plates 500 - 3000, with photographic plates
Maximum range covered in one exposure, Å	$\sim$ 200
Mechanical fittings	ISO-KF, ISO-CF

The pumping system allowed reaching an empty cell base pressure of $\sim 10^{-1}$ μbar. The pressure was monitored in a similar way as during the measurements with the SR. The range of c-C_6H_6 pressure used was 5-15 μbar, much lower than the saturation pressure at the temperatures used (70μbar at 210 K, Fray and Schmitt, 2009). The static pressure increased in about 1 μbar during some of the measurements due to air leaks, with a negligible effect on the experiment. A decrease in radiation intensity was observed due to solid deposits on the windows. This limited the exposure time and, therefore, resolution (as a wider slit was needed to satisfy S/N requirements). The windows of the lamp and cell were regularly cleaned to overcome this problem.

A LAUDA Ultra-Kryomats RUL 80(-D) was in charge of keeping the system at a desired temperature. This latter quantity was measured as for the experiment with SR. The temperature uncertainty was 1 K and the stability better than this. There was no temperature gradient across the cell. During measurements at low temperature (below $\sim$250 K), a heating loop was installed around the entrances of the absorption cell, to avoid air leakage due to the vacuum o-rings becoming rigid.

A measurement series to obtain one c-C_6H_6 absorption spectrum at a particular pressure and temperature, was performed by recording subsequently an empty cell, a sample, and a second empty cell spectrum. The exposure time for each of these spectra was 8 min. Then a dioxygen spectrum was acquired for wavelength calibration purposes, measured using a thinner entrance slit, with an exposure time of 30 min. The photosensitive image plates were then read on a Scanner Cyclone Plus Storage Phosphor System (Perkin-Elmer). The image plates were scanned by the system's laser, focused to less than 43 microns, and the latent image was detected by its optics to create a

high resolution, 16-bit, digitized image with quantitative data. The pixel values were proportional to the flux received. The resulting image contained stripes of some 9000 x 200 (spectral x spatial) pixels, corresponding to the different spectra measured during a measurement series. These stripes were cut, and the rows averaged to get a spectrum (vacuum, benzene or dioxygen). Unexposed regions in the plate were used to estimate a background correction.

The wavelength calibration was performed by using the Schumann-Runge molecular dioxygen absorption bands (1750 - 1950 Å), measured with a resolving power of 50000. The reference spectrum used is from Yoshino et al. (1992), 20 reference points were taken in the range 1750 - 1880 Å. The first-order calibration polynomial determined was used to wavelength-calibrate the benzene spectra. Finally, as this procedure resulted in a shift of the order of 10^{-2} Å between the spectra, they were shifted with respect to the one measured at 215 K, to make the maximum of all spectra coincide.

Tilts, image deformations, and image plate defects, that could produce unreal features in the spectra, were accounted for during processing. The spectra were over-sampled at some 80 points/Å, and binned to achieve 7 points per resolution. A full-range spectrum was created from the two spectra from the image plates, the gap between the plates (some 5 Å in the worst case) was filled with linear interpolated values. As the source flux varied with time during the measurements, and assuming a linear decay in intensity, an average vacuum spectrum was calculated from the the two wavelength-calibrated vacuum spectra. Transmission was calculated in the range 1700 - 1900 Å, from the ratio of the benzene and vacuum intensities. The absorption cross section was derived from this transmission (see below).

Different series of spectra were measured in this experiment, at different temperatures. At least 3 different pressures were explored for a given temperature, confirming reproducibility and pressure independence of the results. Twelve spectra were obtained, arranged in sets, each composed of spectra measured with different pressures but the same temperature. The absorption cross section spectra in each set were then averaged to obtain a final spectrum at the given temperature. The resulting spectra are listed in Table 3.

2.3. Absorption cross section derivation and uncertainties

From the transmission spectra, the absorption cross section was calculated using the Beer-Lambert law in the form

$$T = \frac{I}{I_0} = \exp(-\tilde{\sigma} l \frac{p}{T} \frac{T_0}{p_0}), \quad (1)$$

where the transmission as a function of wavelength, T, is the ratio of the sample spectrum I to the vacuum spectrum I_0, as explained in the previous section. The absorption cross section is $\tilde{\sigma}$, in units of amagat^{-1} cm^{-1}. The optical path through the absorption cell is l; p and T are the pressure and the temperature in the cell, respectively; $T_0 = 273.15\ K$, and $p_0 = 1013.25 \times 10^3 \mu$bar. The absorption cross section presented in the following sections was calculated according to

$$\sigma = \tilde{\sigma}/n_0, \quad (2)$$

where σ is in units of cm^2, and n_0 is the Loschmidt constant $2.6867805 \times 10^{19} cm^{-3}$.

It is very difficult to obtain acceptable absorption measurements in a whole wavelength range where the absorption varies significantly. Low gas pressure in the absorption cell would allow clear measurements of strong absorption regions, but noisy measurements in regions of weak absorption, where the latter could not be clearly determined. High gas pressures in the cell would allow measurements of smaller absorption coefficients, but might saturate strong absorption features. In the range 1700 - 1900 Å the benzene absorption cross section vary by a factor larger than 12. The region around maximum absorption was given priority in this work. As a result, the measurements from the Meudon experiment above 1840 Å are very noisy. Nevertheless, the whole measured range was kept to provide a comparative value with the measurements performed with the SR source. The sources of uncertainty involved in a measurement series include counting statistics from the PM or from the sensitive screen, uncertainty in the values of the optical path, and the values of temperature. But the main and most important source of uncertainty in the derived cross sections is due to the uncertainty in the actual pressure inside the cell. For a particular spectrum the uncertainty was calculated as the relative difference between absorption cross sections measured at two extreme pressures (i.e. two extreme transmissions), and is given by

$$\delta\sigma_\lambda = \frac{\sigma_{\lambda,plow} - \sigma_{\lambda,phigh}}{\sigma_{\lambda,plow} + \sigma_{\lambda,phigh}}, \quad (3)$$

where *plow* and *phigh* represent the lowest and highest pressures measured, respectively, in the wavelength range considered. This resulted in different uncertainty associated to different spectra and wavelength regions, according to different experimental conditions. For spectral regions where

only one pressure was available, the uncertainty could be estimated from measurements in neighboring wavelength regions, and/or measurements at similar temperatures. Table 2 summarizes the uncertainties corresponding to each spectra presented, the limits of the wavelength regions indicated are approximate.

Table 2: Uncertainties corresponding to each spectra derived in this work, and presented in Table 3. The limits of the wavelength regions indicated are approximate.

Absorption cross section uncertainty (%) for measurements with deuterium lamp source				
Temperature (K)	Wavelength range (Å)			
	1710 - 1740	1740 - 1830	1830 - 1910	
295, 245, 215	10	5	20	
Absorption cross section uncertainty (%) for measurements with SR source				
Temperature (K)	Wavelength range (Å)			
	1150 - 1360	1360 - 1600	1600 - 1800	1800 - 2040
298	4	7	3	3
250	<14	<14	<14	
230			7	

Finally, it is worth mentioning that the instrumental bandwidth was greater than the line width (see for example Pantos et al., 1978) of the Rydberg transitions. Therefore, the absorption cross section values for the peaks in the spectra are in these cases underestimated due to this experimental constraint. The valence transitions measured, much broader, do not suffer from this problem.

3. Absorption cross section results and interpretation

The characteristics of the final spectra are presented in Table 3.

Table 3: List of measured spectra. Spectra from the bibliography shown in Figure 2 are also included for reference.

Reference	Temperature (K)	Range (Å)	Resolution (Å)
This work, SR	298	1203 - 2103	1
This work, ^2H	295	1715 - 1911	1
This work, SR	250	1153 - 1600	1
This work, ^2H	245	1715 - 1912	1
This work, SR	230	1723 - 1823	1
This work, ^2H	215	1715 -1912	1
Pickett et al. (1951)	298	1538 - 2119	n[a]
Hammond and Price (1955)	298	1610 - 2130	n[a]
Pantos et al. (1978)	293 - 300	1780 - 2530	2.5
Rennie et al. (1998)	298	348 - 1342	1.7 - 2.3

[a] n = not specified

Figure 2 shows the absorption cross section measured at 298 K, covering the full wavelength range studied. The borders of the wavelength range of the FUV channel of the UVIS instrument, used to

retrieve hydrocarbon density profiles, are shown with dashed lines. In the following we will identify

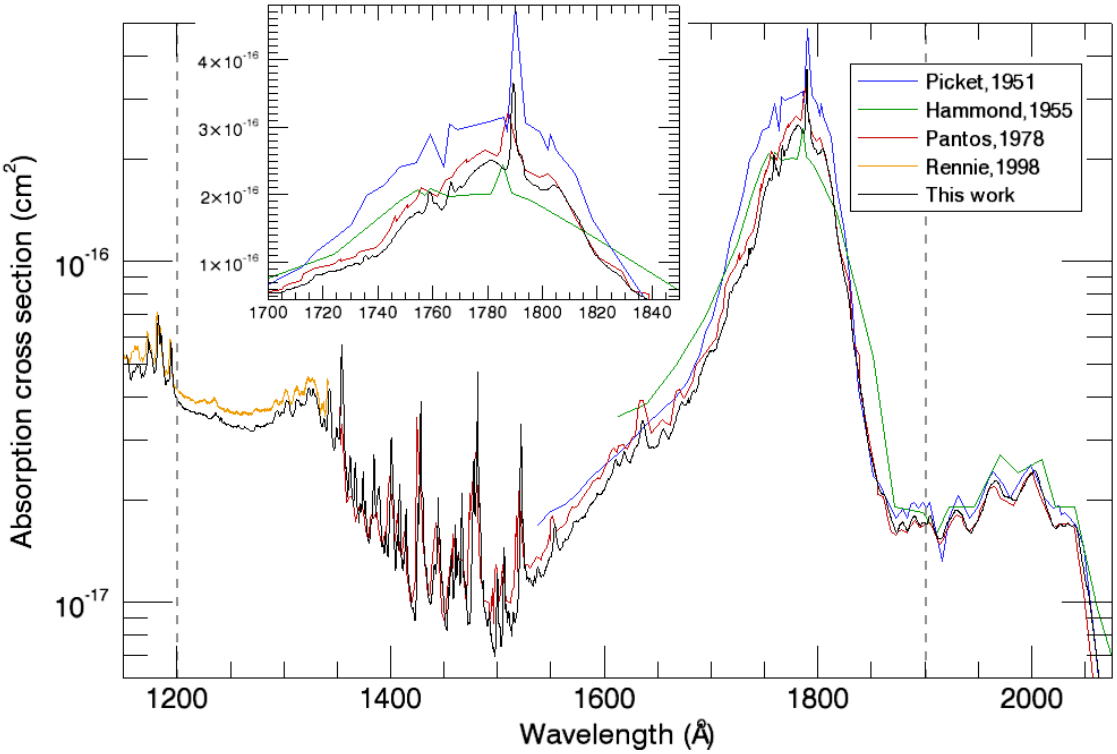

Figure 2: Benzene absorption cross section measured with SR as a source, at 298 K. Measurements from other work are shown for comparison (see text for references). The inset shows the most relevant region for benzene detection in Titan, with the UVIS instrument. The wavelength range of the FUV channel of the UVIS instrument used to retrieve hydrocarbon density profiles is shown as dashed lines.

some of the transitions in our measured spectrum and compare them with previous work, but our intention is not to provide a thorough interpretation of the benzene absorption bands—this has been done before. Nevertheless, our data provide new experimental material that can be used for that interpretation. Our focus is on the general absorption features in the measured spectrum, in the range relevant for the FUV channel of the UVIS instrument (1115 - 1900 Å), their variations with temperature, and their use to identify benzene in Titan's upper atmosphere.

As can be seen in Figure 2, it is difficult to identify band system onsets in the spectrum, due to the overlapping of the neighboring systems and the presence of a continuum. In VUV spectroscopy of polyatomic molecules, valence shell transitions mix with transitions to higher excited

states, in which the excited electrons occupy diffuse Rydberg orbitals with large principal quantum numbers. Even at the moderate resolution of our measurements, however, some band systems and transitions can be identified. Benzene absorption in the wavelength region studied here is 3 order of magnitude stronger than in the region around 2500 Å, where forbidden transitions are located (see for example Fally et al., 2009). This explains the steep decrease of the absorption cross section above 2050 Å. The spectrum in Figure 2 may be divided into 4 regions. The first of these is a diffuse absorption region in 2050 - 1850 Å. The second is a very strong absorption region ranging from 1850 to 1600 Å. The third region of absorption lies below 1600 Å until approximately 1350 Å. It is characterized by strong, narrow Rydberg transitions converging to the first ionization energy (IE) of benzene. Below 1350 Å, the fourth region presents strong bands which are thought to be the first Rydberg bands leading to the second ionization potential of benzene. The absorption for shorter wavelengths corresponds to other Rydberg states (see for example Rennie et al., 1998) converging to higher ionization energies.

In the region 2050-1850 Å, there is a system of very diffuse bands, responsible for the absorption of maximum around 1980 Å. The absorption in the region from 2000 to 1800 Å was interpreted in two different ways (see Pickett et al. (1951); Herzberg (1966) and references therein). It was believed by Carr and Stuecklen (1939) and Hammond et al. (1950) to constitute the first member of the second Rydberg series previously reported by Price and Wood (1935) and co-workers. It has also been associated with the forbidden transition $^1A_{1g} \rightarrow {}^1B_{1u}$ (see for example Feng et al., 2002; Koch and Otto, 1972). The vibrational structure in this region is interpreted as a ring-breathing vibration by Pickett et al. (1951).

The region 1850 - 1600 Å presents an extremely strong, broad absorption with a few sharp peaks and an underlying continuum. It was believed by Pickett et al. (1951) to represent two transitions, a Rydberg series overlying a valence π electron transition of type $^1A_{1g} \rightarrow {}^1E_{1u}$ (Herzberg, 1966; Pantos et al., 1978)—this is the only symmetry-allowed transition in the D_{6h} point group (Hammond and Price, 1955). The peak at 1789.45 Å in our spectrum (1789.09 Å in Pantos et al., 1978, 1790 Å in Pickett et al., 1951, 1786.52 Å in Koch and Otto, 1972), and the accompanying sharp bands were suggested to represent the first member of the second Rydberg transition in Price and Wood

(1935), converging to the first ionization energy of 9.24378 eV [1] (1341.27 Å). Price and Walsh (1947) were convinced about this assignment both by the position of the band and by its accompanying vibrational pattern. They also suggested the overlaying continuous hump of absorption to come from C-H dissociation (also suggested by Nordheim et al., 1940). The 'shoulders' with maxima around 1781 Å and 1804 Å in our spectra were confirmed by Koch and Otto (1972) to be part of the underlying valence transition.

The narrow bands in the region region 1600 - 1350 Å get weaker and closer to each other towards shorter wavelengths, and merge into an absorption continuum at the IE. The sharp bands in this region have been assigned to Rydberg series with their corresponding vibrations (see for example Price and Wood, 1935; Herzberg, 1966; Pantos et al., 1978; Grubb et al., 1985). Some of the series converge to the first IE, others to the second IE at 11.45 eV (1083 Å). The intensity of some of these Rydberg series definitely points to the fact that they are due to allowed transitions of symmetry $^1A_{1g} \rightarrow {}^1E_{1u}$ (Nordheim et al., 1940).

The spectral features in the region 1350 - 1150 Å were already seen by Price and Wood (1935). They are considerably more diffuse than those at wavelengths longer than 1360 Å. Koch and Otto (1972) identified, with the help of photoelectron spectra from Turner (1970), that the groups of bands seen in our spectra are the first (n=3, the group close to 1350 Å) and second (n=4, the group close to 1150 Å) members of a Rydberg series and associated vibrations, converging to the second ionization energy. The first band in the long wavelength end of this region is clear in our spectrum (at about 1355 Å). In a later publication Koch and Otto (1976) identified other Rydberg series, with a first member in the long wavelength structure (1320.39 Å), and a second member at shorter wavelengths (1232.45 Å), also visible in our measurements. This series converges to the third ionization energy, found at 11.71 eV (1060 Å Koch and Otto, 1976). This region has been remeasured and interpreted with the aid of photoelectron spectra by Rennie et al. (1998).

Pantos et al. (1978) underlined the importance of the effect of the instrumental bandwidth. The Beer-Lambert law is correctly used to obtain the cross section only when the exciting light bandpass is much less than the intrinsic line width of an absorption line. This is the case for the $^1A_{1g} \rightarrow {}^1B_{1u}$ transition, for which they found no significant variation with bandwidth, and for the $^1A_{1g} \rightarrow {}^1E_{1u}$

[1] NIST Chemistry WebBook. http://webbook.nist.gov/cgi/cbook.cgi?ID=C71432&Units=SI&Mask=20#Ion-Energetics, January 2015

transition. But for the Rydberg bands our bandwidth was larger than the widths of the lines (line widths of $\sim$ 0.1 Å should be expected in the Rydberg region according to Pantos et al., 1978). In these cases the derived absorption cross sections are underestimated. This is not expected to affect the identification of benzene on Titan in the UVIS observations, because the identification is mostly based on the large feature associated to the $^1A_{1g} \rightarrow {}^1E_{1u}$ valence transition. However, in our spectrum measured at 215 K (see Section 3.1), the peak at 1789.45 Å, associated to the first member of the second Rydberg series in Price and Wood (1935), is about 1.7 times bigger than the maximum of the valence transition. Thus, for the detection of benzene with a higher resolution than that of the UVIS instrument, the effect of this peak in the detection, as well as the dependence of the peak with bandwidth, should be further explored, and attention should be paid to the resolution of the absorption cross section used.

Figure 2 shows results from four other studies (Pickett et al., 1951; Hammond and Price, 1955; Pantos et al., 1978; Rennie et al., 1998). Tabulated data from the first, second and fourth reference were downloaded[2] already in the units plotted here. Data from the third reference was read from their Fig. 3. For the first three references, extinction coefficients have been read from the original work and converted to absorption cross sections (conversion factor 3.8235×10^{-21}). The absorption cross section presented in Suto et al. (1992) and measured at 1 Å resolution (not shown here) agree with those from Pantos et al. (1978) within the 10% uncertainty in the newer results. Improved resolution in our work permits to identify vibrational features absent in the old spectra, particularly the bands around 1759 Å and 1767 Å. The best agreement in absolute value is with the data from Pantos et al. (1978). The ratios of the maximum value in our spectrum over the maxima in the spectra from the references are 0.76, 1.49, and 1.13, for the values from Pickett et al. (1951); Hammond and Price (1955), and Pantos et al. (1978), respectively. The relative difference between our maximum and those in the references are in all cases bigger than the 3% uncertainty in our measurements. There are small shifts in wavelength between our spectrum and those in the references, probably due to the reading process or the higher resolution in our data. A more detailed comparison of the spectra is out of the scope of the present work. Nevertheless, it is clear that our measurements make a significant contribution for the interpretation and applications of the absorption spectrum of benzene.

[2]Downloaded from http://www.atmosphere.mpg.de/, 2014

3.1. Temperature variations

One of the main motivations of this work was to study the response of the benzene absorption cross section to temperature variations. From the pure spectroscopic point of view, even at the moderate resolution of our measurements, it is useful to see the reaction of the different band systems when lowering the temperature. Besides, the knowledge about the variation of the absorption cross section with temperature is of primary importance for atmospheric VUV spectroscopy. In our particular case, the interest focuses in absorption cross sections measured at temperatures relevant for the upper atmosphere of Titan ($\sim$ 150 K, see Cui et al. (2009); Snowden et al. (2013)), or in the confirmation of the absence of significant variations with temperature, at least at the resolution of UVIS. Pickett et al. (1951) mentioned that the relative intensity of the first two bands in the 2000 Å region (reading the spectrum from the long wavelength end), measured at 253 K, showed no measurable change with respect to the measurements at room temperature. Apart from this comment, we found no systematic study of temperature variations of the benzene absorption cross section in the VUV region studied here. For these reasons we measured absorption at different temperatures, and analyzed the variation in the absorption cross sections as a function of temperature.

Figure 3 shows spectra at two different temperatures (298 and 250 K) for the range 1390 - 1490 Å. The figure shows that some bands get narrower and increase in height when the temperature decreases, while other local maxima decrease. This behavior was expected, since collision rates decrease and lower ro-vibronic levels get more populated when the temperature decreases. Some bands representing weaker transitions, at the sides of a stronger one, decrease with decreasing temperature. These correspond to transitions from higher vibrational energy levels, whose population decreases with decreasing temperature, and consequently the intensity of the associated absorption. Although some of the variations observed correspond to real changes with temperature, variations of the position of the maxima in wavelength which are smaller than the 0.17 Å measurement precision (see Section 2.1) should not be taken into account.

Spectra at different temperatures for the range 1700 - 2050 Å are shown in Figure 4. The difference in the region 1715 - 1820 Å, between the measurements performed at room temperature with the two different instruments described in Section 2, is less than 10% (less than 5% for most of the wavelength range). This is an indication of the repeatability of the measurements. Indeed, both spectra were measured at almost the same temperature, with the two different experimental setups

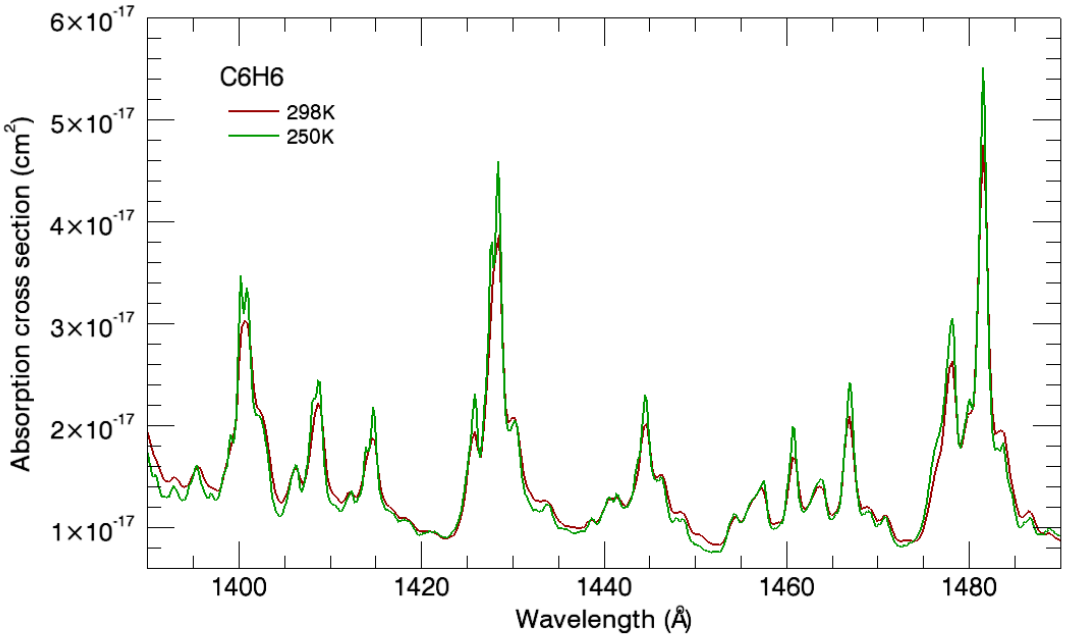

Figure 3: Benzene absorption cross section measured at two different temperatures, 298 K and 250 K, in the range 1390 - 1490 Å.

presented; the fact that the residual is within the limits of the uncertainty in the measurements verifies the coherence of the results, and validates further comparison of results derived from the different experiments.

The curves for 245, 230, and 215 K in Figure 4 present a common overall behavior. The absorption cross section decreases with decreasing temperature in most of the wavelength range 1730 - 1820 Å (shown in the inset of Figure 4). The biggest decrease is observed for wavelengths at the local minima in the absorption cross section. For some of the local maxima the behavior is opposite, the absorption increasing with decreasing temperature, while the width of the associated bands diminishes. This is evident for the local maxima around 1760 Å (only for the 230 K curve) and for the global maximum in the region, close to 1790 Å. These variations with temperature are consistent with the explanations in terms of population of levels given above. Even though most of the observed variations with temperature remain within the measurement uncertainty (see Table 3), some significant variations (greater than the uncertainty) as a function of temperature are observed. These include the variation of the maximum close to 1790 Å. Other significant variations are seen

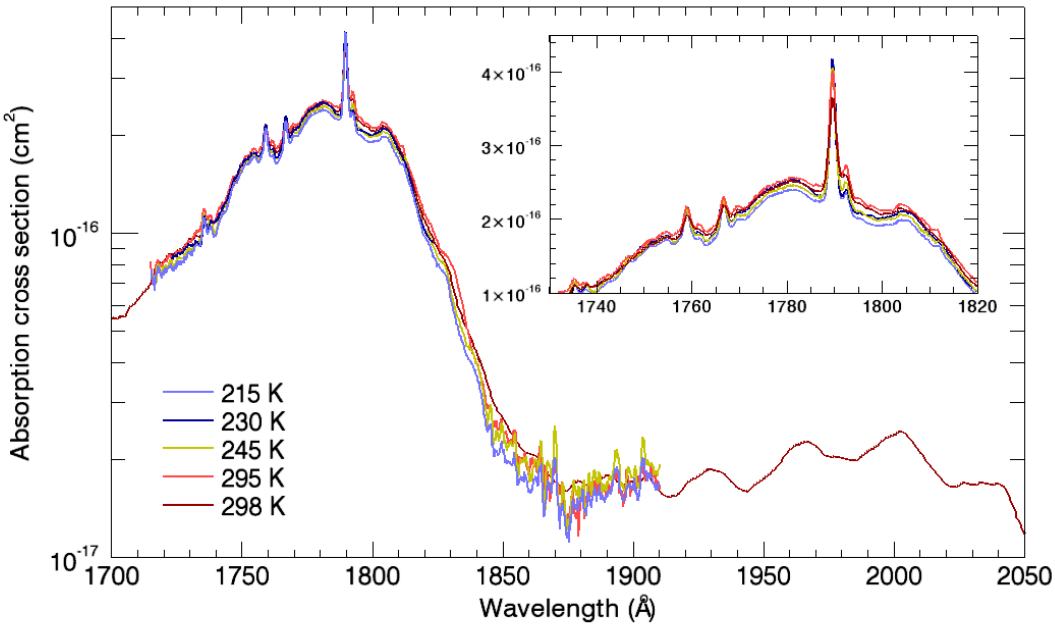

Figure 4: Benzene absorption cross section at different temperatures, in the range 1700 - 2050 Å.

for some of the minima, particularly, the minimum around 1791.5 Å. These variations around the minima are more evident for the curve corresponding to measurements at 215 K.

The identification of benzene in the UVIS spectrum is based on the $^1A_{1g} \rightarrow {}^1E_{1u}$ intense absorption, and to lesser extent on the over-imposed Rydberg peaks. Significant variations with temperature, of up to 10% (14% in the Rydberg maximum), are observed within this spectral range. The relative uncertainty in the transmission measured by UVIS in this region, for altitudes of 650 km and 800 km, is around 6 to 15%. Therefore, effects on the retrieval of benzene on Titan with UVIS due to variations of the absorption cross section with temperature could, in principle, be relevant (we show in Section 5,however, that the effects are within the uncertainty in the number density), and the absorption cross section measured at 215 K should be used. On the other hand, 215 K is the lowest temperature explored here, while Titan's thermosphere can be as cold as ∼120 K (see for example Snowden et al., 2013). However, going from 215 to 120 K, the population of the vibrational ground state increases by $\sim$ 18%. The corresponding change between 298 K and 215 K is $\sim$ 26%, and the variation in absorption cross section about 10 %, as commented above. The

change in the absorption cross section between 215 K and 120 K is then expected to be less than 8%. Therefore, an influence on the c-C_6H_6 retrieval from UVIS data, caused by a temperature effect on the absorption cross section is not expected in this case, and the use of absorption cross section measured at 215 K is justifiable for the analysis.

4. Analysis of stellar occultation observed by UVIS

This section describes briefly the data and methods used to derive atmospheric composition. This was done by combining absorption cross sections from laboratory measurements, and stellar occultations measured with the far ultraviolet (FUV: 1115 - 1913 Å) channel of the UVIS instrument, aboard the Cassini spacecraft. For a more detailed description of the instrument and its data see Esposito et al. (2004). More information and details about the occultation technique, VUV occultations, data, and data reduction (including geometrical calculations and the retrieval procedure) can be found in Koskinen et al. (2011); NASA-PDS (2012); Capalbo (2014), and references therein.

4.1. Atmospheric composition from absorptive VUV stellar occultations

During occultations the spectrum of the star is observed along different lines of sight through the atmosphere. These spectra are divided by the unattenuated spectrum observed outside of the atmosphere, to obtain transmission. The measured transmission is determined by the absorption of the different species at different altitudes. Absorption is the dominant phenomena for the observations analyzed here, although extinction from aerosols is also considered. Ultraviolet airglow from Titan's atmosphere (Ajello et al., 2007, 2008), scattered radiation into the instrument FOV, and refraction effects can be neglected (Koskinen et al., 2011).

This work focuses on benzene. The other molecules considered to perform the retrieval of abundances are CH_4, acetylene (C_2H_2), hydrogen cyanide (HCN), ethylene (C_2H_4), diacetylene (C_4H_2), cyanoacetylene (HC_3N), and aerosols (AER). These have already been identified in the FUV spectrum of Titan (Shemansky et al., 2005; Koskinen et al., 2011). Our choice of molecules was also founded on an analysis of theoretical detectability of different species based on their absorption cross section, their model-predicted abundances in the atmosphere, as well as UVIS resolution and S/N (Capalbo, 2014). The absorption cross sections of the molecular species (other than benzene, see Section 3) and the extinction cross sections of aerosols, used in the retrieval

of atmospheric constituents, can be found in Koskinen et al. (2011) and Capalbo (2014). The molecular absorption cross sections were measured in laboratory, the extinction cross sections for the aerosols were calculated for spherical aerosols with a radius of 100 Å, using Mie theory and assuming the optical properties of tholins (Khare et al., 1984; Koskinen et al., 2011). This choice is irrelevant to the task of separating aerosols from the other absorbers.

For each tangent altitude (i.e., the shortest distance from the line of sight to the surface of Titan), the column densities were determined from comparisons of modeled transmission with measured transmission. The column densities are inverted to obtain number density profiles. These inversion problems are generally ill-posed. So, the column density profiles were retrieved using a χ^2-minimization technique, and the number density profiles were retrieved using a constrained linear inversion method. Very similar procedures have been used before to analyze occultations (Vervack et al., 2004; Quemerais et al., 2006; Koskinen et al., 2011) and the technique presented here follows them closely. A detailed step by step explanation of the procedure is given in Capalbo (2014), a summary of the procedure follows.

4.1.1. Column density retrieval

In order to separate different absorbers, and to retrieve their column densities, we fitted the transmission spectra at each tangent altitude. The model used to fit the data involved the absorption cross sections of the species considered and a convolution with the instrument response, that we modeled as a Gaussian with a 2.38 Å width and two lorentzians, one of width 34.44 Å, the other of width 392.35 Å (See the UVIS User's guide NASA-PDS, 2012). In the general case, the absorption cross sections (or extinction cross section for the aerosols) depend on temperature, and consequently on altitude. In this work the absorption cross section were considered independent of altitude, absorption cross sections measured at low temperatures were used when available. The optimal column densities were determined by using the Levenberg-Marquardt (see for example Press et al., 1996) minimization algorithm with the IDL routine MPFIT (Markwardt, 2009), wrapped in an iteration scheme to work around unphysical values, that can result from the non-convergence of the routine to a minimum.

To exclude meaningless results in the extremes of the altitude range (due to transmission values very close to one or to zero), the column density profiles were restricted in altitude. The valid altitudes in the profile of a particular species were defined as those for which the transmission was roughly between 0.01 and 0.99, for wavelength regions where the species has characteristic

absorption. Outliers and abundances for which MPFIT could not provide a value and a consistent uncertainty, were replaced by interpolated values, assuming a decreasing exponential behavior as a function of altitude. Interpolated values in the final column density profiles remain rare: only 1 to 10 altitudes, normally in the lower or upper boundaries of the profiles, and mainly for HCN, HC_3N, c-C_6H_6, and AER. No values were extrapolated.

4.1.2. Number density and aerosol extinction retrieval

The number densities were determined by using a constrained inversion of the column density profiles, or Tikhonov regularization (see for example Quemerais et al., 2006). The constraint was based on the assumption of smoothness of the solution, and implemented via a second derivative operator. The intensity of the regularization is given by the regularization parameter Λ. The determination of Λ is key in the process, and several criteria are possible. A small value of Λ would result in a noisy profile. If Λ is too big, too much smoothing will produce a featureless profile. The details of our implementation of the Tikhonov algorithm are in Capalbo (2014). The resolution of the retrieved profiles are determined by the so-called averaging kernel matrix.

Some of the values in the retrieved profile are not shown because the inversion failed to provide a reasonable value and uncertainty. These values are in most cases in the minima, or the the lower altitudes of the number density profiles. Moreover, values within one resolution width from the top of the profiles were eliminated, to account for a border effect due to the second derivative operator used in the inversion. The different points in the profile have similar but different altitude resolutions. The median of the resolutions is reported as a characteristic resolution for the whole profile. The routines developed to retrieve the number densities from the measured transmission were validated with simulated data as described in Capalbo (2014).

4.1.3. Uncertainties and benzene identification

There are several sources of uncertainties associated with the analysis. The uncertainty coming from the Poisson counting statistics in the detector is propagated in the calculation of transmission and optical depth. The MPFIT routine provides the 1-σ uncertainties of the column densities, determined from the spectral fit. The uncertainties in the number densities are evaluated by means of a formal error propagation through the inversion routine. The systematic uncertainty coming from the measured absorption cross sections (up to 10% in the worst cases), are not included in the final uncertainties. Our analysis based on simulated data shows that the uncertainties from MPFIT

are often underestimated. However, the analysis showed that, for most of the altitudes, the 'true' number density profiles were retrieved to within 2-σ. Thus, we recommend the 2-σ uncertainty interval to be used when interpreting the results in Section 5.

The retrieval techniques used to derive the density profiles of the species are based on their absorption cross section. But the technique itself is unable to identify a molecule given an absorption cross section spectrum, the identity of the molecule is determined by the 'user'. This is based not only on the confidence that the absorption cross section used corresponds to the molecule of interest, but also on the confidence on the correlation of features in both the absorption cross section, and the measured spectrum. The question might then arise about the true identity of a particular species, particularly when isotopic substitution, or substituted molecules (like substituted benzenes), can lead to absorption spectra similar to that of the molecule of interest. The sets of absorption bands obtained in both light and heavy benzene are essentially similar (Price and Wood, 1935; Rennie et al., 1998). However, those of the latter suffer a small shift to the violet relative to those of the former. Moreover, the H/D ratio measured for Titan by different techniques is about 10^{-4} (Table 10.4 in Soderblom et al., 2009). Other benzene derivatives present absorption cross sections similar to that of benzene (see for example Hammond et al., 1950; Suto et al., 1992). But the main valence transition, and the over-imposed Rydberg transition around 1790 Å in the benzene absorption cross section (see section 3), that actually determine its presence in the UVIS FUV spectrum, is shifted in the benzene derivatives by more than the UVIS spectral resolution (except maybe for benzotrifluoride, which is irrelevant for studies of Titan's atmospheric chemistry). Moreover, the abundance of more complex aromatic rings is expected to be lower than that of benzene and, thus, also their contribution to absorption. All this strongly suggests that the species we retrieved using the absorption cross section presented in this work is, indeed, benzene.

4.2. UVIS observations analyzed

Geometric and other ancillary information about the stellar occultations analyzed in this work is presented in Table 4. The geometry of observation was calculated with the help of the SPICE information system and the SPICE toolkit, from the Navigation and Ancillary Information Facility (NAIF, Acton, 1996). The integration duration for each spectrum, the spacecraft velocity and attitude, determined the vertical sampling of the atmosphere. The integration time was 1.75 s for the stellar occultations analyzed here, the sampling of the atmosphere varied slightly from one occultationto the other, between 0.5 and 4 km. The altitude sampling was, after altitude averaging

Table 4: Characteristics of the stellar occultations analyzed.

Flyby	Data product (FUV <yyyy_doy_hh_mm>)	Star	Lat. (deg) [a]	Lon. (deg W) [a]	Atmosp. in shadow [a]	Altitudes probed (km)	Original sampling (km) [a]	S/c - TA min. [b] (km) [a]
T21	FUV_2006_346_10_39	α Eri	-35 – -36	116 – 119	no	0 – 2330	3.8	1.6×10^4
T41	FUV2008_054_15_36	ϵ CMa	-2 – -10	332 – 334	yes	243 – 2000	0.4	4.7×10^5
T41_II	FUV2008_054_21_31	ϵ CMa	-24 – -28	173 – 175	no	72 – 3044	0.8	6.0×10^5
T53	FUV2009_109_21_23	α Eri	38 – 39	294 – 308	no	0 – 4627	1.6	3.8×10^4

[a] for altitudes relevant to absorption measurements

[b] Spacecraft - tangent altitude minimum distance

to improve S/N, around 10 km. The final vertical resolution was determined by the number density retrieval process (see section 4.1). Although the reflection of light by the atmosphere and UV airglow are negligible for a 1-2 s exposure, it is still useful to know if the atmosphere probed by the occultation was in shadow or not. This information is given in the sixth column of Table 4.

During the data reduction process, the dark current of the instrument and the background (determined from the counts measured low in the atmosphere, where no photons from the source are expected to reach the detector) were negligible. The effect of low response ('evil') pixels in the detector was corrected by linear wavelength-interpolation (see UVIS User's Guide, NASA-PDS (2012)). For the occultation data products analyzed in this work, 5 rows in the detector corresponds to useful data, the corresponding rows were summed up. The result is a 2-D matrix containing count values for wavelength-time (or tangent altitude) coordinates.

Four occultations were analyzed in this work: T21, T41, T41_II, and T53. These were chosen because of their pointing stability, and because our results from T41 and T53 can be compared with those derived previously for these flybys (Koskinen et al., 2011), with an almost identical technique. The profiles derived cover altitudes roughly from 350 to 1200 km, which lies in between of those covered by CIRS and INMS. In general, the span in longitude and latitude for the relevant altitudes is only a few degrees. Hence, the profiles derived from UVIS data can be considered as real vertical profiles. The star occulted during flybys T21 and T53 was Alpha Eridani (Achernar), the star occulted during flybys T41 and T41_II was Epsilon Canis Majoris (Adara).

5. Titan's atmospheric composition

5.1. Previous results from UVIS FUV stellar occultations

Stellar UVIS FUV occultations by Titan were first presented by Shemansky et al. (2005). From the occultations measured during flyby Tb, they derived column density profiles for CH_4, C_2H_2,

HCN, C_2H_4, C_2H_6, and C_4H_2. The observations covered altitudes from 450 to 1600 km above the surface. The C_4H_2 absorption cross sections used by Shemansky et al. (2005) were saturated at 1445 Å and 1645 Å, which might have led to an overestimation of the abundance for this species. Liang et al. (2007) used the same UVIS data from the Tb flyby to detect and characterize aerosols, at altitudes between 500 and 1000 km. The detection of aerosols in this region implies that they are formed at higher altitudes in the thermosphere. The results of Koskinen et al. (2011), based on occultations T41 and T53, significantly expanded on the previous analysis of UVIS FUV occultations. They led to the identification of new absorbers in the data (C_6H_6 and HC_3N), the detection and characterization of aerosol layers in the upper atmosphere, the retrieval of detailed density profiles for 7 gaseous species, and the detection of large scale waves in Titan's mesosphere. Capalbo (2014) included a thorough analysis and characterization of the retrieval techniques to derive composition from UVIS FUV stellar occultations. In the present work, the technique was applied to data from flybys T21, T41, T41_II, and T53. We present new c-C_6H_6 profiles, obtained for the first time with the absorption cross sections measured at low temperature (see Section 3). We note that the density profiles are obtained simultaneously for all 8 absorbers, but here we limit our focus on benzene.

5.2. Column densities and residuals

We obtained column density profiles for all the species included in the model, and for the 4 occultations. As the minimum of the cost function depends on the line of sight abundance of all the species, none of them can be assessed independently, and the output of the spectral fit as a whole has to be taken into account. The quality of the column densities obtained can be estimated from the value of the reduced χ^2 (χ^2_R) and the residuals between the model and the observations. The χ^2_R is the value of the χ^2 quantity divided by the degrees of freedom (number of wavelength channels contributing to χ^2 minus the number of parameters). The χ^2_R fell for most of the altitudes in the range 0.85 - 1.45 for T21, the ranges were 0.7 - 2.6 for T41, 1.0 - 2.0 for T41_II, and 0.8 - 1.8 in the case of T53. These values imply a good fit. The normalized residuals are the difference between the modeled transmission (computed from the retrieved column densities) and the measured transmission, divided by the uncertainty in the measured transmission. The residuals for flybys T21 and T41_II are shown in Figure 5. As the quality of the fit varies with altitude, a species in the model could be missing or underestimated (positive residual), or overestimated (negative residual), for some altitudes. The residuals shown, as examples, correspond

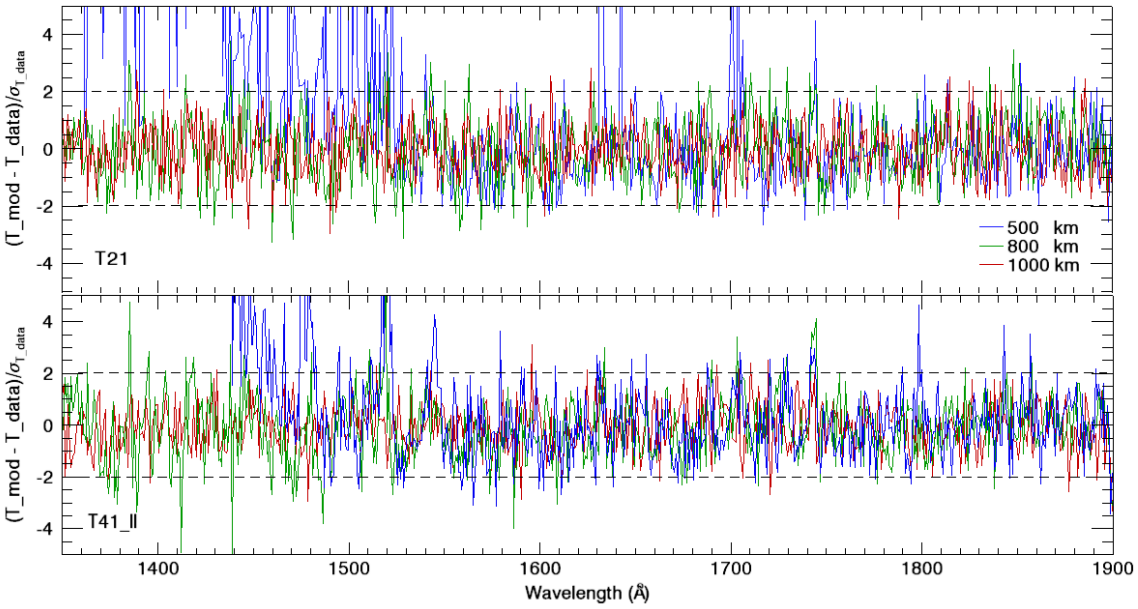

Figure 5: Normalized transmission residuals for 3 altitudes, from flybys T21 and T41_II. The residuals for T41 and T53 present similar characteristics.

to altitudes 500, 800 and 1000 km. A thorough analysis of the residuals is out of the scope of the present work. However, some characteristics are worth mentioning. According to the tests of performance of the retrieval technique, only residuals larger than 2-σ are significant. Isolated peaks, at individual wavelengths, are not interpreted as coming from an absorbing species. Below 600 km the transmission below ∼1500 Å (and for some individual values around 1630 Å and 1700 Å in the case of T21) is practically zero, and the calculated residual has no physical significance. The same happens below 800 km and wavelengths below 1350 Å. The discrepancies around 1520 Å is likely related to the strong C_2H_2 absorption feature, and might indicate an underestimation of this species at the two altitudes concerned. A similar comment apply to the discrepancies around 1540 Å, that could indicate a slight underestimation of C_4H_2. The discrepancies around 1690 and 1700 Å, and those around 1730 and 1740 Å, might indicate a small underestimation of C_2H_4. The discrepancies mentioned were also observed in Koskinen et al. (2011). The residuals for T41 and T53 have similar characteristics as those shown in Figure 5. On the whole, there is no clear sign of significant residuals that might indicate a missing species in the model; the column densities obtained are considered to describe well the state of the atmosphere at the different altitudes. The

column density profiles of benzene are shown in Figure 6.

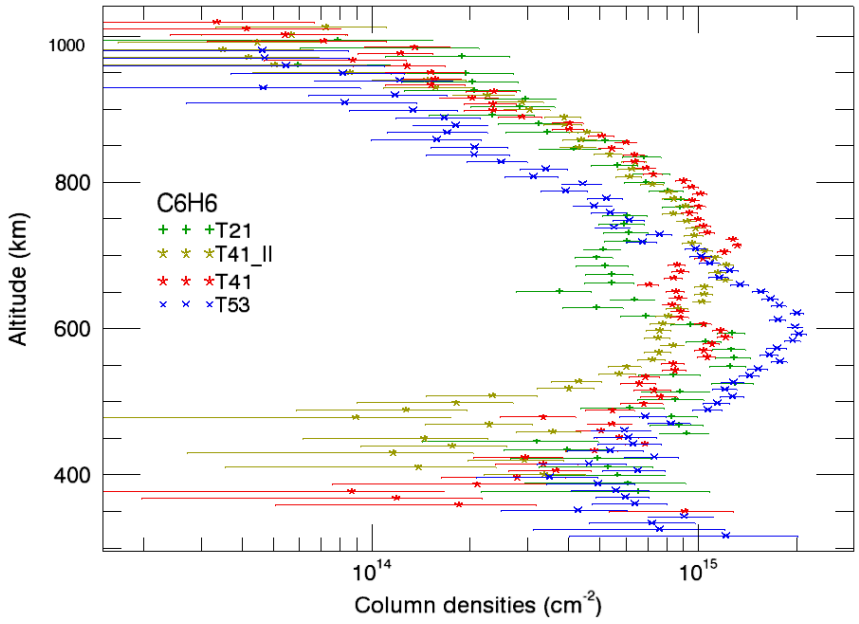

Figure 6: Benzene column density profiles, for the 4 stellar occultations analyzed. Horizontal bars show the 1-σ uncertainties.

5.3. Benzene number densities

We obtained number density profiles for all the species included in the model, and for the 4 occultations. The number density profiles for C_6H_6 in the upper atmosphere of Titan are plotted in Figure 7. Oscillations of about 15-20% in number density and a few tens of km should be interpreted with caution, as might be due to divergences from the real profile caused by the noise in the column densities, not smoothed by the regularization procedure. The altitude resolution of the number density profiles depends on the width of the averaging kernels (which in turn depends on the amount of regularization or smoothing applied by the retrieval process), and on the effective atmospheric sampling (after altitude averaging)(Capalbo et al., 2013). The resolutions are 60 km, 20 km, 20 km, and 25 km for T21, T41, T41_II, and T53, respectively.

Benzene profiles in the upper atmosphere, derived from UVIS observations during flybys T41 and T53 have been presented by Koskinen et al. (2011). In this case, the retrieval was performed with a now outdated version of the room temperature c-C_6H_6 absorption cross sections presented here. For most of the altitudes, the values presented here differ from those in Koskinen et al. (2011)

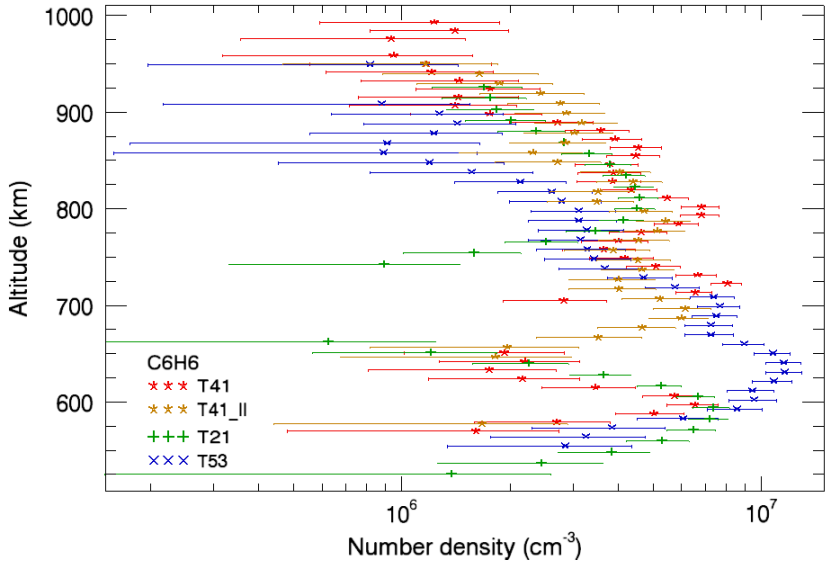

Figure 7: Benzene number density profiles from the 4 occultations analyzed. Horizontal bars show the 1-σ uncertainties.

in less than twice the uncertainty (or 2σ) in our results. The exception are 2 values (one at 600 km and the other at 800 km), for which the difference is still smaller than 3σ. The use of updated and low temperature benzene absorption cross section is one of the reasons for the small differences observed in the c-C_6H_6 (and other species) profiles from the two analyses.

The benzene profiles from different occultations in Figure 7 agree for some altitudes, but they also present marked differences for some others. Among the most evident, is the much smaller abundances derived from the T53 flyby, above roughly 750 km. This is not the case between roughly 600 and 660 km, where the profile from T53 is bigger than the others by a factor bigger than 5. The profile from T53 is the latest measured (April 2009), and is the only one which was measured in the northern hemisphere (39°). The profile from T21 follows the general trend of those from T41 and T41_II above 750 km, although much smoother, and the trend of the profiles from T41 and T53 below 600 km. But the benzene abundance from T21 is much smaller than that in the other flybys between 650 and 750 km. The shape of the curve points to a very low minimum that could not be handled by the inversion routines, leaving a gap of data for some altitudes. The profile from T21 is the first (December 2006), and the most southern of the 4 measured (-39°). A very low minimum, like that in the T21 profile, could also be present between 650 and 700 km in

the case of T41. This kind of depletion could lead to the inversion routine failure, responsible of the almost complete lack of values below 650 km for T41_II. These depletion regions are also evident, though much more subtle, in the column densities (see Figure 6). Finally, the profile from T41 and T41_II present more oscillations above 700 km than the profiles from the other occultations. The profile from T41 has maxima at the same time (or separated by about one altitude resolution) that the profile from T41_II has minima. On the other hand, the 2σ envelope of the profiles overlap for most of the altitudes. Moreover, we remind that small oscillations (like the one near 740 km in the profile from T41_II) could be artifacts of the retrieval. The differences we observe between equatorial (T41) and low southern latitude (T41_II) observations are of a factor 2.4 at most, both observations taking place with a few hours difference. It has to be noted that T41 is a night occultation, and the T41_II occultation was measured during the day. So diurnal, and not only latitudinal, variability should also be taken into account when interpreting these differences.

The differences between the profiles could be due to geographical and/or temporal variability of benzene in the upper atmosphere. Latitudinal variations of benzene abundances in the stratosphere have been reported by Vinatier et al. (2010), from the analysis of CIRS data measured during northern winter (2005 - 2007). Vinatier et al. (2015) reported temporal variations in the benzene mixing ratios, from the analysis of CIRS data measured during a longer period (2006 - 2012), including the northern Spring equinox. However, the measurements derived from CIRS for the stratosphere, where benzene abundances depend strongly on latitude, are not directly comparable with our values for the thermosphere. The few observations presented here prevent an analysis of benzene variability in these upper layers, which is out of the scope of the present paper. Nevertheless, the information presented can set the basis for this kind of studies, in combination with other observations, in future publications.

5.3.1. Effect of variations of absorption cross sections with temperature

To see the effect of the small variations with temperature in the absorption cross section of benzene (see Section 3) in the number density profile, the retrieval was performed with benzene absorption cross sections at room temperature, and the number densities compared with those obtained using low temperature absorption cross sections. This was done for two test occultations: T41 and T53. The number densities retrieved using the absorption cross section measured at room temperature are slightly lower. This can be explained by the fact that, although the maximum at 1790 Å is bigger for low temperatures, the overall valence transition is smaller. A relative difference

profile was calculated as the difference between the profiles derived with absorption cross sections at different temperatures, divided by the uncertainty. The mean of this relative difference profile is 0.4 (for T41), and 0.3 (for T53). For all altitudes, the relative difference is smaller than 2 (smaller than 1 for T53). So, the effect of the small variations in the absorption cross sections with temperature is negligible for the detection of benzene on Titan with UVIS. Curiously, the profiles of HC_3N and C_2H_4 are sensitive to the variation in the c-C_6H_6 absorption cross sections, with variations of up to 2-σ for some altitudes (although the mean of the relative differences in the profile is close to zero for these species). This could be due to the overlapping of the C_2H_4 and the c-C_6H_6 absorption cross section between 1700 and 1850 Å. In the case of HC_3N, although its identification does not depend on its absorption cross section in this wavelength range, it might be influenced by the change in C_2H_4. The other species were not significantly affected.

5.3.2. Comparison with models and observations

To compare our results with other measurements and models of benzene abundance in Titan, we converted our number densities into mixing ratios. For this, we used the atmospheric mass density profile measured by the the Huygens Atmospheric Structure Instrument (HASI, Fulchignoni et al., 2005), after expressing it as number density, assuming an atmosphere composed of 98.52% of N_2, and 1.48% of CH_4 (Niemann et al., 2010). The 10% uncertainty in the HASI profile was taken into account to calculate the uncertainty in the mixing ratios. As commented before, UVIS FUV stellar occultations probe a region in the atmosphere below that probed by INMS, and above the region probed by CIRS. A detailed comparison with profiles derived from these instruments is not part of the objectives of this work, and therefore we limit our comparison to some values. Figure 8 shows our profiles together with measurements by INMS (Cui et al. (2009), shown as Cui09, and Magee et al. (2009), Magee09 in the plot), and CIRS (Vinatier et al. (2015), shown as vinatier15). Magee et al. (2009) derived neutral composition of Titan's upper atmosphere from the analysis of 20 Titan flybys. These took place from October 2004 till May 2008. Cui et al. (2009) studied composition and thermal structure of the upper atmosphere based on the analysis of INMS data from 15 Titan flybys, spanning 2.5 years, from April 2005 till November 2007. The values derived from INMS shown in Figure 8 correspond to global average mixing ratios of C_6H_6. These values are more than an order of magnitude smaller than our highest values, which lay only some tens of km below those from INMS. Figure 8 is consistent with Figure 26 in Koskinen et al. (2011), that also compares benzene mixing ratios derived from INMS and CIRS, with those from UVIS measurements during

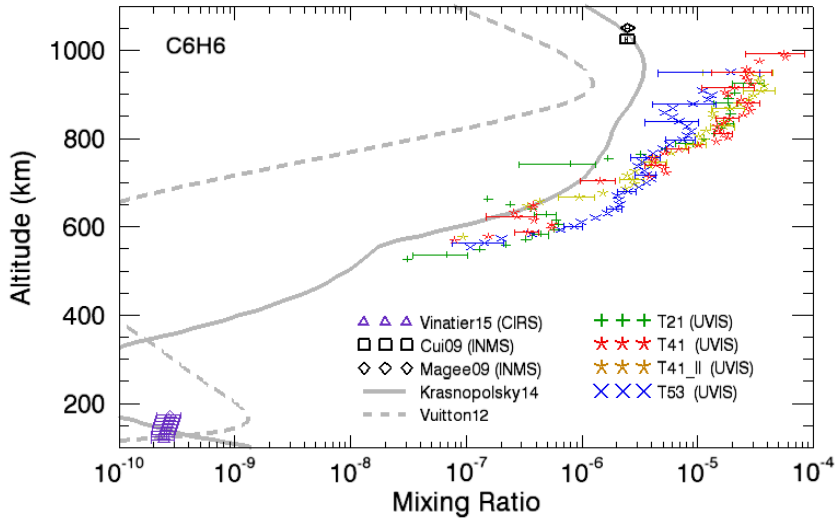

Figure 8: Benzene mixing ratios derived from stellar occultations measured by UVIS, only some uncertainty bars are shown for clarity. Also shown are profiles from models (Vuitton et al., 2012; Krasnopolsky, 2014)), INMS observations (Cui et al., 2009; Magee et al., 2009), and CIRS observations (Vinatier et al., 2015).

T41. In addition, we show here 3 other profiles derived from UVIS occultations. Although spatial or temporal variability could be hypothesized to explain the differences between the results from UVIS and those from INMS, the fact that all of the profiles derived from UVIS give larger benzene mole fractions than the INMS data makes this hypothesis unlikely.

The difference between INMS results and UVIS results raises the question of the reliability of the two methods (mass spectrometry and UV spectroscopy). Although INMS results are subject to absolute calibration uncertainties, the instrument measures both N_2 and C_6H_6, and the ratio should be accurately determined. The density profiles from occultations are more accurate than the INMS densities because they are independent of absolute calibration, but the mixing ratio determination needs to assume an N_2 density profile. We used the HASI density profile (the only profile measured 'in-situ' reaching the lower altitudes probed by UVIS), which is untypically high when compared to other measurements (see for example Capalbo et al., 2013). Using lower N_2 densities would, however, produce an even larger disagreement between INMS and UVIS. If other species in the atmosphere, non accounted for in our analysis, had extinction characteristics similar to those of benzene in the long wavelength end of the FUV spectrum, the benzene abundance profile derived from the occultations could be overestimated. However, in Section 4.1.3 we presented arguments

against this possibility. The difference observed between INMS results and UVIS results should be further explored in the future.

The benzene profile derived from CIRS shown in Figure 8 (Vinatier et al., 2015) is from the T16 flyby, on July 2006, and corresponds to a latitude of 46°N, and a longitude of 110°W. This was chosen because, being the lowest latitude profile in the cited reference, should be closest to the global average. Moreover, it is close in time to the T21 UVIS observation analyzed here. Although the inclusion of the profile derived from CIRS is useful to provide a general picture of benzene abundances, the gap of about 350 km between this profile and those from UVIS, the fact that the values correspond to different times and locations, and the variability of benzene observed in the CIRS data, make it difficult to compare the observations without a more detailed analysis of the behavior of benzene in the stratosphere, out of the scope of the present work (see for example Vinatier et al., 2015).

Figure 8 also shows benzene profiles from photochemical models: a profile from Vuitton et al. (2012)(from the model called 'C' in the paper), shown as Vuitton12, and a profile from Krasnopolsky (2014), shown as Krasnopolsky14. Vuitton et al. (2008) proposed a formation of benzene via $C_6H_7^+$ electron recombination near 900 km, which is the main formation region; and from neutral radical reaction in the stratosphere. Benzene is then rapidly depleted by photolysis, and suffers a rapid decrease below 900 km. The model in Vuitton et al. (2008) was constrained with INMS and CIRS data, the resulting C_6H_6 mole fraction profiles reproduced well the measurements of these instruments around 1000 km and 100 km, respectively. Vuitton et al. (2012) presented an improved model in which they calculated radiative association reaction rates using transition state theory. They found that, with the new changes in the model, mole fractions can vary by as much as one order of magnitude locally. The dashed grey line in Figure 8 is a profile from the model in Vuitton et al. (2012). The maximum in the curve at about 923 km is roughly one order of magnitude smaller than the measurements, the difference being more than two orders of magnitudes for lower altitudes. The oscillations in the measurements are missed in the model.

Krasnopolsky (2014) compared results from his photochemical model and different observations, for different species, including C_6H_6. They found that the model reproduces the observational data, within variations comparable to the uncertainty in the measurements and the differences between different measurements. The solid grey line in Figure 8 represents the C_6H_6 mixing ratio profile in their model. The calculated profile reproduces the general trend of increasing abundance with

altitude, but falls short of the values derived from UVIS data by a factor of about 5 in the lowest altitudes, and a factor of about 8 in the highest altitudes. Oscillations in the measured profiles are not reproduced by the model. It is worth mentioning that, in the two models used for the comparison, the profiles are calculated for global average conditions (applicable to low and mid latitudes), solar zenith angle of 60°, and photolysis rates reduced by a factor 2 (to account for the night side). Thus, comparisons with observations at specific time of the day, latitude, and longitude, should be done with caution. Moreover, the large scale oscillations in the measured profiles might be caused by atmospheric waves, not included in the models. Furthermore, the photochemical models are subject to several uncertainties including those in reaction rates. On the whole, although the models reproduce the general trend of mixing ratio increasing with altitude, the data indicate that the models do not produce enough benzene to match the UVIS occultations. Our results imply that the benzene chemistry needs to be re-evaluated.

6. Conclusions

The knowledge of the benzene absorption cross section is mandatory for its detection with UVIS. The absorption cross sections have been thoroughly explored in the past, but an analysis of their temperature dependence was lacking, and presented in this work. We presented absorption cross sections in the range 1153 - 2103 Å, at 1 Å resolution. We show, for the first time, absorption cross sections in the range 1720 - 1820 Å for 4 different temperatures in the range 215 - 298 K. The measurements are self consistent, and compare well with previous work, apart from some differences in wavelength and cross section value, possibly due to the higher resolution in our measurements. Not much significant variation of the absorption cross sections with temperature was observed, but some temperature effects could be qualitatively and quantitatively analyzed. This variation affects the derivation of benzene profiles on Titan from UVIS data in less than the 1-σ uncertainty in the profiles. However, the cross sections measured at 215 K should be used for the analysis, to avoid a small systematic shift in abundance of the profiles. No further significant variations in the absorption cross section affecting the retrieval with UVIS are expected at lower temperatures. The spectroscopic data presented in this work are a valuable new addition to the benzene absorption cross section databases. The measurements will become part of a more extensive database of absorption

spectra of molecules of astrophysical interest, available online to the scientific community[3].

The benzene absorption cross sections measured were added to a bigger set of laboratory results, and used to analyze 4 stellar occultations by Titan's atmosphere (T21, T41, T41_II, and T53), observed with the FUV channel of the UVIS instrument. We retrieved column density profiles and number density profiles. Our benzene profiles from T41 and T53, agree well with those in Koskinen et al. (2011), the only previous work that presented this kind of results. They derived benzene profiles from the same occultations, with a similar technique, but an outdated set of absorption cross sections. The four profiles presented here correspond to different times and locations. The differences between each other could, therefore, result from latitudinal or temporal variability of benzene.

The profiles of benzene obtained in the present work cover the altitude gap between the INMS observations and the CIRS observations. Our profiles do not smoothly match globally averaged values derived from INMS. The big difference between INMS values and all 4 UVIS profiles seems unlikely to be explained by temporal or spatial variability. A more thorough comparison should be done to interpret the benzene abundance in the whole altitude range covered by the measurements.

The stellar occultation profiles show a general trend of mixing ratio increasing with altitude, predicted in the profiles from state-of-the-art model calculations. However, in general, the models do not produce enough benzene and fall short of the measurements, and the oscillations in the later are not reproduced by the former. These differences point to complex chemical and, especially, dynamical processes affecting the benzene vertical distribution, revealed by measurements but out of reach by current models. Vertical profiles like the ones derived in this work for benzene, are a fundamental reference to constrain the models, and improve our understanding of Titan's upper atmosphere.

Up to June 2014 we identified 18 stellar occultations measured by UVIS. A preliminary analysis showed that, excluding the four presented here, they present pointing instabilities that make their analysis much more complicated. Although a method has been developed to correct unstable UVIS solar occultations measured with the Extreme Ultraviolet channel (Capalbo, 2014), no such technique has yet been developed for the FUV channel, and remains a challenge for the future. Furthermore, Cassini arrived at the Saturnian system in 2004, and the mission is planned to be

[3]Available at http://www.lisa.univ-paris12.fr/GPCOS/SCOOPweb/lesmoleculesdeSCOOP.htm

continued till 2017. Therefore, some FUV observations during 2 more years are expected to be available. The variability present in current observations could be further examined in the remaining of the Cassini mission, combining observations from different experiments.

7. Acknowledgments

We are grateful for the valuable help received from the staff at the BESSY II synchrotron facility, during our measurements of benzene absorption. We acknowledge the financial support from the French Space Agency (Centre National d'Études Spatiales, CNES). TTK acknowledges support from the NASA CDAPS grant NNX14AD51G.

8. References

Acton, C. H., 1996. Ancillary data services of nasa's navigation and ancillary information facility. Planetary Space Science 44 (1), 65 – 70.

Ajello, J., Gustin, J., Stewart, I., Larsen, K., Esposito, L., Pryor, W., McClintock, W., Stevens, M., Malone, C., Dziczek, D., 2008. Titan airglow spectra from the Cassini ultraviolet imaging spectrograph: Fuv disk analysis. Geophysical Research Letters 35 (6).

Ajello, J., Stevens, M., Stewart, I., Larsen, K., Esposito, L., Colwell, J., McClintock, W., Holsclaw, G., Gustin, J., Pryor, W., 2007. Titan airglow spectra from Cassini ultraviolet imaging spectrograph (UVIS): Euv analysis. Geophysical Research Letters 34 (24).

Bézard, B., Drossart, P., Encrenaz, T., Feuchtgruber, H., 2001. Benzene on the giant planets. Icarus 154 (2), 492 – 500.

Capalbo, F., Bénilan, Y., Yelle, R., Koskinen, T., Sandel, B., Holsclaw, G., McClintock, W., 2013. Solar occultation by titan measured by Cassini/UVIS. Astrophysical Journal Letters 766 (2), (5 pp.).

Capalbo, F. J., 2014. Titan's upper atmosphere composition and temperature from cassini ultraviolet imaging spectrograph stellar and solar occultations. Ph.D. thesis, University of Paris Est.

Carr, E. P., Stuecklen, H., 1939. An electronic transition of the rydberg series type in the absorption spectra of hydrocarbons. Journal of Chemical Physics 7 (8), 631.

Cernicharo, J., Heras, A., Tielens, A., Pardo, J., Herpin, F., Guelin, M., Waters, L., 2001. Infrared space observatory's discovery of c4h2, c6h2, and benzene in crl 618. Astrophysical Journal, Letters 546 (2).

Coll, P., Coscia, D., Smith, N., Gazeau, M.-C., Ramírez, S., Cernogora, G., Israël, G., Raulin, F., 1999. Experimental laboratory simulation of titan's atmosphere: aerosols and gas phase. Planetary and Space Science 47, 1331 – 1340.

Coustenis, A., Achterberg, R. K., Conrath, B. J., Jennings, D. E., Marten, A., Gautier, D., Nixon, C. A., Flasar, F. M., Teanby, N. A., Bézard, B., Samuelson, R. E., Carlson, R. C., Lellouch, E., Bjoraker, G. L., Romani, P. N., Taylor, F. W., Irwin, P. G. J., Fouchet, T., Hubert, A., Orton, G. S., Kunde, V. G., Vinatier, S., Mondellini, J., Abbas, M. M., Courtin, R., 2007. The composition of titan's stratosphere from Cassini/CIRS mid-infrared spectra. Icarus 189 (1), 35 – 62.

Coustenis, A., Salama, A., Schulz, B., Ott, S., Lellouch, E., Encrenaz, T., Gautier, D., Feuchtgruber, H., 2003. Titan's atmosphere from iso mid-infrared spectroscopy. Icarus 161 (2), 383.

Cui, J., Yelle, R., Vuitton, V., Waite, J., Kasprzak, W., Gell, D., Niemann, H., Mueller-Wodarg, I., Borggren, N., Fletcher, G., Patrick, E., Raaen, E., Magee, B., 2009. Analysis of titan's neutral upper atmosphere from Cassini ion neutral mass spectrometer measurements. Icarus 200 (2), 581 – 615.

De La Haye, V., Waite, J. H., J., Cravens, T. E., Robertson, I. P., Lebonnois, S., 2008. Coupled ion and neutral rotating model of titan's upper atmosphere. Icarus 197 (1), 110 – 136.

Delitsky, M. L., McKay, C. P., May 2010. The photochemical products of benzene in titan's upper atmosphere. Icarus 207, 477–484.

Esposito, L. W., Barth, C. A., Colwell, J. E., Lawrence, G. M., Mcclintock, W. E., Stewart, A. I. F., Keller, H. U., Korth, A., Lauche, H., Festou, M. C., Lane, A. L., Hansen, C. J., Maki, J. N., West, R. A., Jahn, H., Reulke, R., Warlich, K., Shemansky, D. E., Yung, Y. L., 2004. The Cassini ultraviolet imaging spectrograph investigation. Space science reviews 115 (1-4), 299 – 361.

Fally, S., Carleer, M., Vandaele, A., 2009. Uv fourier transform absorption cross sections of benzene,

toluene, meta-, ortho-, and para-xylene. Journal of Quantitative Spectroscopy and Radiative Transfer 110 (9), 766 – 782.

Feng, R., Cooper, G., Brion, C., 2002. Dipole (e,e+ion) spectroscopic studies of benzene: absolute oscillator strengths for molecular and dissociative photoionization in the vuv and soft x-ray regions. Journal of Electron Spectroscopy and Related Phenomena 123 (2), 211 – 223.

Ferradaz, T., Bénilan, Y., Fray, N., Jolly, A., Schwell, M., Gazeau, M. C., Jochims, H.-W., 2009. Temperature-dependent photoabsorption cross-sections of cyanoacetylene and diacetylene in the mid- and vacuum-UV: Application to Titan's atmosphere. Planetary and Space Science 57, 10 – 12.

Fray, N., Schmitt, B., 2009. Sublimation of ices of astrophysical interest: A bibliographic review. Planetary and Space Science 57, 2053 – 2080, doi:10.1016/j.pss.2009.09.011.

Fulchignoni, M., Ferri, F., Angrilli, F., Ball, A. J., Bar-Nun, A., Barucci, M. A., Bettanini, C., Bianchini, G., Borucki, W., Colombatti, G., Coradini, M., Coustenis, A., Debei, S., Falkner, P., Fanti, G., Flamini, E., Gaborit, V., Grard, R., Hamelin, M., Harri, A. M., Hathi, B., Jernej, I., Leese, M. R., Lehto, A., Stoppato, P. F. L., López-Moreno, J. J., Maekinen, T., McDonnell, J. A. M., McKay, C. P., Molina-Cuberos, G., Neubauer, F. M., Pirronello, V., Rodrigo, R., Saggin, B., Schwingenschuh, K., Seiff, A., Simoes, F., Svedhem, H., Tokano, T., Towner, M. C., Trautner, R., Withers, P., Zarnecki, J. C., 2005. In situ measurements of the physical characteristics of Titan's environment. Nature 438, doi:10.1038/nature04314.

Grubb, S. G., Otis, C. E., Whetten, R. L., Grant, E. R., Albrecht, A. C., 1985. Higher excited states of benzene: Symmetry assignments of six gerade rydberg series by four-photon absorption spectroscopy. Journal of Chemical Physics 82 (3), 1135.

Hammond, V. J., Price, W. C., 1955. Oscillator strengths of the vacuum ultra-violet absorption bands of benzene and ethylene. Transactions of the Faraday Society 51, 605.

Hammond, V. J., Price, W. C., Teegan, J. P., Walsh, A. D., 1950. The absorption spectra of some substituted benzenes and naphthalenes in the vacuum ultra-violet. Discussions of the Faraday Society 9, 53.

Hebrard, E., Dobrijevic, M., Bénilan, Y., Raulin, F., 2007. Photochemical kinetics uncertainties in modelling Titan's atmosphere: First consequences. Planetary and Space Science 55, 1470 – 1489.

Herzberg, G., 1966. Molecular spectra and molecular structure. Vol. III. Electronic Spectra and Electronic structure of polyatomic molecules. D. Van Nostrand Company Inc.

Imanaka, H., Smith, M. A., Turro, N. J., 2010. Formation of nitrogenated organic aerosols in the titan upper atmosphere. Proceedings of the National Academy of Sciences of the United States of America (28), 12423.

Khare, B., Sagan, C., Arakawa, E., Suits, F., Callcott, T., Williams, M., 1984. Optical constants of organic tholins produced in a simulated titanian atmosphere: from soft x-ray to microwave frequencies. Icarus 60 (1), 127 – 137.

Koch, E., Otto, A., 1972. Optical absorption of benzene vapour for photon energies from 6 ev to 35 ev. Chemical Physics Letters 12 (3), 476 – 480.

Koch, E., Otto, A., 1976. Vacuum ultra-violet and electron energy loss spectroscopy of gaseous and solid organic compounds. International Journal of Radiation Physics and Chemistry 8 (1), 113 – 150.

Koskinen, T., Yelle, R., Snowden, D., Lavvas, P., Sandel, B., Capalbo, F., Bénilan, Y., West, R., 2011. The mesosphere and lower thermosphere of titan revealed by Cassini/UVIS stellar occultations. Icarus 216 (2), 507 – 534.

Krasnopolsky, V. A., 2009. A photochemical model of titan's atmosphere and ionosphere. Icarus 201 (1), 226 – 256.

Krasnopolsky, V. A., 2014. Chemical composition of titan's atmosphere and ionosphere: Observations and the photochemical model. Icarus 236 (0), 83 – 91.

Lavvas, P., Coustenis, A., Vardavas, I., 2008. Coupling photochemistry with haze formation in titan's atmosphere, part ii: Results and validation with Cassini/Huygens data. Planetary & Space Science 56 (1), 67 – 99.

Lebonnois, S., 2005. Benzene and aerosol production in titan and jupiter's atmospheres: a sensitivity study. Planetary and Space Science 53 (5), 486 – 497.

Lebonnois, S., Bakes, E. L. O., McKay, C. P., 2002. Transition from gaseous compounds to aerosols in titan's atmosphere. Icarus 159 (2), 505.

Liang, M.-C., Yung, Y. L., Shemansky, D. E., 2007. Photolytically generated aerosols in the mesosphere and thermosphere of titan. The Astrophysical Journal Letters 661 (2), L199.
URL http://stacks.iop.org/1538-4357/661/i=2/a=L199

Magee, B. A., Waite, J. H., Mandt, K. E., Westlake, J., Bell, J., Gell, D. A., 2009. INMS-derived composition of titan's upper atmosphere: Analysis methods and model comparison. Planetary and Space Science 57, 1895 – 1916.

Markwardt, C. B., 2009. Non-linear least-squares fitting in idl with mpfit. In: Bohlender, D. A., Durand, D., Dowler, P. (Eds.), Astronomical Data Analysis Software and Systems XVIII. Vol. 411. ISBN: 978-1-58381-702-5.

NASA-PDS, 2012. Cassini UVIS User's Guide. PlanetaryDataSystem, http://pds-rings.seti.org/cassini/uvis/index.html.

Niemann, H. B., Atreya, S. K., Demick, J. E., Gautier, D., Haberman, J. A., Harpold, D. N., Kasprzak, W. T., Lunine, J. I., Owen, T. C., Raulin, F., 2010. Composition of titan's lower atmosphere and simple surface volatiles as measured by the cassini-huygens probe gas chromatograph mass spectrometer experiment. Journal of Geophysical Research: Planets 115 (E12), n/a–n/a.
URL http://dx.doi.org/10.1029/2010JE003659

Nordheim, G., Sponer, H., Teller, E., 1940. Note on the ultraviolet absorption systems of benzene vapor. Journal of Chemical Physics 8 (6), 455 – 458.

Pantos, E., Philis, J., Bolovinos, A., 1978. The extinction coefficient of benzene vapor in the region 4.6 to 36 ev. Journal of Molecular Spectroscopy 72 (1), 36 – 43.

Pickett, L. W., Muntz, M., McPherson, E. M., 1951. Vacuum ultraviolet absorption spectra of cyclic compounds .1. Cyclohexane, cyclohexene, cyclopentane, cyclopentene and benzene. Journal of the American Chemical Society 73 (10), 4862–4865.

Press, W. H., Teukolsky, S. A., Vetterling, W. T., Flannery, B. P., 1996. Numerical Recipes in Fortran 90, 2nd Edition. Vol. 2 of Fortran Numerical Recipes. Press Syndicate of the University of Cambridge.

Price, W. C., Walsh, A. D., 1947. The absorption spectra of benzene derivatives in the vacuum ultra-violet. i. Proceedings of the Royal Society of London. Series A, Mathematical and Physical Sciences (1024), 22.

Price, W. C., Wood, R. W., 1935. The far ultraviolet absorption spectra and ionization potentials of c6h6 and c6d6. Journal of Chemical Physics 3 (8), 439.

Quemerais, E., Bertaux, J.-L., Korablev, O., Dimarellis, E., Cot, C., Sandel, B. R., Fussen, D., 2006. Stellar occultations observed by spicam on mars express. Journal of Geophysics Research 111, doi:10.1029/2005JE002604.

Raulin, F., Toupance, G., Mourey, D., 1982. Organic-syntheses from ch_4-n_2 atmospheres: Implications for titan. Origins of Life 12 (3), 267.

Rennie, E., Johnson, C., Parker, J., Holland, D., Shaw, D., Hayes, M., 1998. A photoabsorption, photodissociation and photoelectron spectroscopy study of c6h6 and c6d6. Chemical Physics 229 (1), 107 – 123.

Sanchez, R. A., Ferris, J. P., Orgel, L. E., 1966. Cyanoacetylene in prebiotic synthesis. Science (3750), 784.

Shemansky, D. E., Stewart, A. I. F., West, R. A., Esposito, L. W., Hallett, J. T., Liu, X., 2005. The Cassini UVIS stellar probe of the titan atmosphere. Science 308 (5724), 978 – 982.

Snowden, D., Yelle, R., Cui, J., Wahlund, J.-E., Edberg, N., Å gren, K., 2013. The thermal structure of titan's upper atmosphere, i: Temperature profiles from Cassini INMS observations. Icarus 226 (1), 552 – 582.

Soderblom, L. A., Barnes, J. W., Brown, R. H., Clark, R. N., Janssen, M. A., McCord, T. B., Niemann, H. B., Tomasko, M. G., 2009. Titan from Cassini-Huygens. Springer, Ch. 10.

Suto, M., Xiuyan, W., Jun, S., Lee, L., 1992. Quantitative photoabsorption and fluorescence spectroscopy of benzene, naphthalene, and some derivatives at 106-295 nm. Journal of Quantitative Spectroscopy and Radiative Transfer 48 (1), 79 – 89.

Turner, D. W., 1970. Molecular phoroelectron spectroscopy, a handbook of the 584 Åspectra. Wiley.

Vervack, J. R. J., Sandel, B. R., Strobel, D. F., 2004. New perspectives on titan's upper atmosphere from a reanalysis of the voyager 1 uvs solar occultations. Icarus 170 (1), 91 – 112.

Vinatier, S., Bézard, B., Nixon, C. A., Mamoutkine, A., Carlson, R. C., Jennings, D. E., Guandique, E. A., Teanby, N. A., Bjoraker, G. L., Flasar, F. M., Kunde, V. G., 2010. Analysis of Cassini/CIRS limb spectra of titan acquired during the nominal mission. i. hydrocarbons, nitriles and co2 vertical mixing ratio profiles. Icarus 205, 559 – 570.

Vinatier, S., Bózard, B., Fouchet, T., Teanby, N. A., de Kok, R., Irwin, P. G., Conrath, B. J., Nixon, C. A., Romani, P. N., Flasar, F. M., Coustenis, A., 2007. Vertical abundance profiles of hydrocarbons in titan's atmosphere at 15 s and 80 n retrieved from Cassini/CIRS spectra. Icarus 188, 120 – 138.

Vinatier, S., Bzard, B., Lebonnois, S., Teanby, N. A., Achterberg, R. K., Gorius, N., Mamoutkine, A., Guandique, E., Jolly, A., Jennings, D. E., Flasar, F. M., 2015. Seasonal variations in titan's middle atmosphere during the northern spring derived from cassini/cirs observations. Icarus 250 (0), 95 – 115.

Vuitton, V., Doussin, J.-F., Bénilan, Y., Raulin, F., Gazeau, M.-C., 2006. Experimental and theoretical study of hydrocarbon photochemistry applied to titan stratosphere. Icarus 185 (1), 287 – 300.

Vuitton, V., Yelle, R. V., Cui, J., 2008. Formation and distribution of benzene on titan. Journal of Geophysical Research 113 (E5), E05007.

Vuitton, V., Yelle, R. V., Lavvas, P., Klippenstein, S. J., 2012. Rapid association reactions at low pressure: Impact on the formation of hydrocarbons on titan. The Astrophysical Journal 744 (1), 11.

Vuitton, V., Yelle, R. V., McEwan, M. J., 2007. Ion chemistry and n-containing molecules in titan's upper atmosphere. Icarus 191 (2), 722 – 742.

Waite, J.H., J., Niemann, H., Yelle, R., Kasprzak, W., Cravens, T., Luhmann, J., McNutt, R., Wing-Huen, I., Gell, D., De La Haye, V., Muller-Wordag, I., Magee, B., Borggren, N., Ledvina,

S., Fletcher, G., Walter, E., Miller, R., Scherer, S., Thorpe, R., Jing, X., Block, B., Arnett, K., 2005. Ion neutral mass spectrometer results from the first flyby of titan. Science 308 (5724), 982 – 986.

Wilkinson, P. G., 1956. Absorption spectra of benzene and benzene-d6in the vacuum ultraviolet. Canadian Journal of Physics 34 (6), 596.

Wilson, E., Atreya, S., 2003. Chemical sources of haze formation in titan's atmosphere. Planetary & Space Science 51 (14/15), 1017.

Wilson, E. H., Atreya, S. K., Coustenis, A., 2003. Mechanisms for the formation of benzene in the atmosphere of titan. Journal of geophysical research 108 (E2), 8.1 – 8.10.

Wilson, E. H. b. a., Atreya, S. K., 2004. Current state of modeling the photochemistry of titan's mutually dependent atmosphere and ionosphere. Journal of geophysical research 109 (E6), E06002.1 – E06002.39.

Yoshino, K., Esmond, J., Cheung, A.-C., Freeman, D., Parkinson, W., 1992. High resolution absorption cross sections in the transmission window region of the schumann-runge bands and herzberg continuum of o2. Planetary and Space Science 40 (2), 185 – 192.